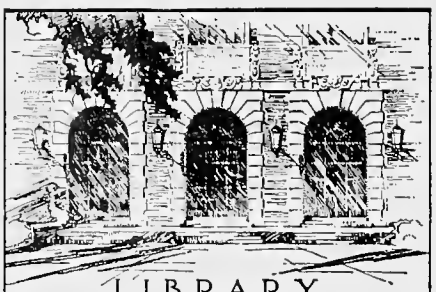

AFCRL 64-653

UNIVERSITY OF ILLINOIS
URBANA

AERONOMY REPORT NO. 3

GYRO-INTERACTION ROCKET EXPERIMENTS IN THE LOWER IONOSPHERE

by
Ralph Richard Hodges, Jr.

November, 1964

epared for
r Force Cambridge Research Laboratories
fice of Aerospace Research
nited States Air Force
dford, Massachusetts

Antenna Laboratory
Department of Electrical Engineering
Engineering Experiment Station
University of Illinois
Urbana, Illinois

AFCRL 64-653

GYRO-INTERACTION ROCKET EXPERIMENTS IN THE LOWER IONOSPHERE

by

Ralph Richard Hodges, Jr.

November 1964

Aeronomy Report No 3

Contract AF19(628)-3900
Project 8605
Task 860505

AIR FORCE CAMBRIDGE RESEARCH LABORATORIES
OFFICE OF AEROSPACE RESEARCH
UNITED STATES AIR FORCE
LAURENCE G. HANSCOM FIELD
BEDFORD, MASSACHUSETTS

Antenna Laboratory
Department of Electrical Engineering
Engineering Experiment Station
University of Illinois
Urbana, Illinois

Requests for additional copies by agencies of the Department of Defense, their contractors, or other government agencies should be directed to:

DEFENSE DOCUMENTATION CENTER (DDC)
CAMERON STATION
ALEXANDRIA, VIRGINIA 22314

Department of Defense contractors must be established for DDC services or have their "need-to-know" certified by the cognizant military agency of their project or contract.

All other persons and organizations should apply to the:

U. S. DEPARTMENT OF COMMERCE
OFFICE OF TECHNICAL SERVICES
WASHINGTON, D. C. 20230

ABSTRACT

Two gyro-interaction rocket experiments have been performed in the lower ionosphere. The basic experimental procedure consists in the radiation of periodic pulses of gyrofrequency energy from a transmitter within the rocket payload. The effect of each pulse is to produce a sudden disturbance of electron energy near the rocket. This may be accompanied by increased electron density due to collisional ionization or detachment. The rate at which each disturbance relaxes to equilibrium is measured by a cross-modulation technique. To do this a CW sensing wave is transmitted from the ground and detected at the rocket. Its path traverses the disturbances; modifications of the permittivity of the disturbed regions produce the cross-modulation.

With the use of this technique, rate coefficients for two processes have been evaluated. With a strong gyrofrequency pulse the local electron density is increased. The rate of removal of these excess electrons, which is believed to be due to attachment, has been determined in the range of 45 to 65 km. When the gyrofrequency pulse is weak, the disturbance is only a slight increase of electron energy. This increases the collision frequency and hence affects the absorption of the sensing wave. The rate of loss of excess electron energy has been determined by this method. At altitudes above the sensing wave reflection level cross-modulation of plasma noise has been detected.

An RF probe, with which the frequency dependence of the real part of the input impedance of an antenna was detected, was included in one experiment to measure electron density and collision frequency. In addition the data confirms some of the theoretical implications of Balmain's work. The device has been designated a real impedance probe.

ACKNOWLEDGEMENT

The author wishes to express deep appreciation to his adviser, Professor G. A. Deschamps, for encouragement and guidance in this work. Thanks are also due to Professor L. Goldstein who first proposed the gyro-interaction rocket experiment and who participated in the initial formulation of experimental techniques along with Professors Mast and Mittra, Dr. Balmain, and Mr. Shubert. The assistance of Messrs. Fowler, Henry, and Hudock in designing of various experimental components was invaluable. In addition it is a pleasure to acknowledge the efforts of Messrs. Flaherty, Hanchett, Liang, Maiman, Mayberry, Wissmiller, and others of the Antenna Laboratory and of the Special Services staffs in the Department of Electrical Engineering of the University of Illinois in the instrumentation of rocket payloads and ground support equipment.

Special thanks are also due the Collins Radio Company for its contribution of a 10 KW broadcast transmitter for use in a ground support role in these experiments.

It is also a pleasure to acknowledge the assistance which has been received of Mr. Ulwick and other personnel of the Air Force Cambridge Research Laboratories and its contractors in the preparation and launching of the rockets. Thanks are also due the many individuals of the Eglin Air Proving Ground Center who participated in these launchings and in subsequent data processing.

This research has been sponsored by the Air Force Cambridge Research Laboratories under contracts AF19(604)-3481, AF19(604)-5565, AF19(628)-2484, and AF19(628)-3900, and by the Defense Atomic Support Agency under WEB 04.054.

TABLE OF CONTENTS

LIST OF ILLUSTRATIONS

LIST OF ILLUSTRATIONS (continued)

1. INTRODUCTION

Knowledge of the rate coefficients associated with the various atmospheric processes is essential to the task of explaining the composition and behavior of the upper atmosphere. Of particular interest are those processes which involve electrons and hence affect the propagation of radio waves in the ionosphere.

While the rate coefficients for specific processes may be studied in the laboratory, the state of knowledge of the ionosphere permits some speculation as to which processes are dominant. Thus there is a need for study of these processes by means of direct measurements in the ionosphere. In recent years the availability of sounding rockets for ionospheric research has made this possible.

In this investigation rockets were used in making in situ measurements of some rate coefficients for processes involving electrons. In a manner similar to the Luxembourg effect the experimental technique made use of the interaction of electromagnetic fields with the magnetoplasma properties of the ionosphere. Two payloads have been instrumented and launched. The essential results from these experiments and their interpretations are the objects of this report.

2 THE MEASUREMENT OF RATE COEFFICIENTS BY WAVE INTERACTION

A rate coefficient indicates how fast a quantity returns to its equilibrium value after being disturbed. Thus one means of measuring a rate coefficient is to produce an excess of the quantity in question and then to observe it as a function of time as it relaxes.

For example the diurnal variations of ionospheric electron density are in part the result of the changing degree of solar radiation. In the transition from day to night the rate of ionization decreases; the rates of disappearance of electrons from the various regions then depend on corresponding rates of recombination, attachment, and diffusion. The study of the faster rate coefficients requires a more abrupt change or disturbance of some quantities, such as is provided naturally by a solar eclipse or more dramatically by a high altitude nuclear explosion. Obviously a specific process can be studied only if the disturbance or the measuring apparatus is sufficiently selective to distinguish between the several processes involved.

Those processes which affect the distribution of electrons in the ionosphere are of major importance. These also are the most easily studied since electron energy can be modified by the application of strong electric fields and measured by means of weak sensing fields.

A classic example of the exploitation of this fact is the Luxembourg effect which was reported by Tellegen[1] in 1933 and subsequently explained by Bailey and Martyn[2] in 1934. Involved is a collisional process in which a strong RF signal with amplitude modulation interacts with the electrons of the ionosphere causing variations in their energy (or temperature) at the modulating frequency Temporal changes are thus produced in the electron collision frequency and hence in the refractive index of the disturbed region. Weaker signals refracted in this time-varying medium receive the modulation of the

strong disturbing signal. This process is called cross-modulation. In the literature the weaker signal has been designated a sensing or wanted wave; the stronger a heating or disturbing signal.

Numerous experiments using this technique have been performed in investigations of the lower ionosphere. Among these are measurements of collision frequency ν and electron energy loss rate $G\nu$ by Bailey et al.,[3] Fejer,[4] Fejer and Vice,[5] and Rumi.[6] The interaction of radio waves was extended to laboratory plasmas using guided microwaves by Professor Goldstein and coworkers[7] in 1953. This has made possible the study of various processes in atmospheric gases under controlled conditions. A recent review of work in this area has been published by Narasinga Rao, Verdeyen, and Goldstein.[8]

3. GYRO-INTERACTION EFFECTS

A free electron moving in a DC magnetic field is acted upon by a force proportional to the cross product of its velocity with the DC magnetic induction B_o. As this force is perpendicular to B_o, the transverse motion (with respect to B_o) of the electron is in a circular orbit. For nonrelativistic speeds the period of each cycle is independent of velocity; the inverse of this period, known as the gyrofrequency or cyclotron frequency, is given by

$$f_H = \frac{|e\ B_o|}{2\pi\ m} \tag{3.1}$$

If a gyrofrequency electric field is applied, circularly polarized in the same sense as the orbital motion of the electron, the force on the electron will be constant throughout each cycle. Thus the gyrofrequency field is equivalent to a DC electric field with $B_o = 0$ The result is a linear increase of transverse electron velocity with time.

Obviously a field at any frequency other than f_H would not remain in synchronism with the orbiting electron; hence, electron energy would oscillate rather than steadily increase. However, if the electron makes a collision with a neutral gas molecule, much of the ordered energy gained from the field is converted into thermal energy (i.e., increased electron temperature). There is a band of frequencies about f_H in which the synchronism of the field with the electron orbital motion lasts longer than the mean time between collisions. This is called the gyroresonance. It has a width of roughly twice the collision frequency. The heating of electrons, and hence the absorption of energy from the field, is thus much more effective within the gyroresonance than at other frequencies.

A second effect near the gyrofrequency is the increase of collision frequency due to the increase of electron temperature. As a result the resonance width increases and the rate of absorption of energy from the field decreases. Thus, gyro-interaction involves both the heating of electrons and the decreasing of absorption near the gyrofrequency.

Noting the gyroresonance Bailey[9] in 1938 predicted that cross-modulation in Luxembourg effect experiments should exhibit a resonance when the strong disturbing signal is swept through the gyrofrequency. This was experimentally verified by Cutolo[10] in 1950 and by Bailey et al.[3] in 1952. The high absorption of the gyrofrequency energy results in a layer of heated electrons which may be very thin, depending on the gradient of electron density in the ionosphere during the experiment. For this reason some experimenters have avoided the gyrofrequency when interest lay in probing the ionosphere over a range of altitudes(references 4, 5, and 6 are examples).

Gyro-interaction has been used extensively by Professor Goldstein and his students[8] in laboratory cross-modulation experiments. The success of this work led Professor Goldstein to propose in 1959 that ionospheric processes be studied by cross-modulation techniques with the use of a gyrofrequency transmitter carried in a rocket.

With a pulsed gyrofrequency transmitter in a rocket the surrounding electrons can be heated regardless of altitude. The high absorption of gyrofrequency energy produces a localized disturbance of electron energy. Measurements of the rate of relaxation of each disturbance can be made at the rocket and the results related to rate coefficients at specific altitudes

In the rocket experiment there is some latitude in the type of disturbance which can be produced A weak gyrofrequency pulse may increase electron

temperature slightly over a region with dimensions of several wavelengths. A strong pulse, however, could produce sufficient electron energy to cause an increase of electron density very near the rocket. The mechanism of electron production could be collisional detachment at lower altitudes where the ratio of negative ions to electrons is high; at higher altitudes ionization, similar to antenna breakdown, could occur. If electron density were increased, the rate of loss of electron energy would be much faster than that for removal of excess electrons. Thus the two processes might be observed separately in some altitude ranges.

4. EXPERIMENTAL PROCEDURE

In the course of this study two rockets have been instrumented and launched. The basic procedure in both experiments was that indicated schematically in Figure 1. A gyrofrequency transmitter within the rocket emits periodic pulses, each of which produces increased electron temperatures in some localized region near the rocket. A cw sensing wave at 2.02 Mc is transmitted from the ground, traverses the disturbed region, and is detected at the rocket by a receiver. To the extent that a disturbance modulates the sensing wave the relaxation rates of the processes involved in returning the disturbed region to equilibrium can be obtained from the receiver output. This information is telemetered and recorded at the ground.

As the terrestrial magnetic field is a function of altitude, the operating frequency for the so-called gyrofrequency transmitter is not the exact gyrofrequency over the entire flight. Since the width of the gyroresonance is twice the collision frequency, it is only necessary that the operating frequency be within this bandwidth over the range of altitudes of interest. At Eglin Air Force Base, Florida, where these experiments have been performed, the sea level magnetic induction B_o is 5.276×10^{-5} webers meter^{-2}. With the use of an inverse cube approximation for the decrease of magnetic field with distance from the center of the earth, the gyrofrequency

$$f_H = \frac{|e B_o|}{2\pi m} \tag{4.1}$$

is plotted as a function of altitude in Figure 2. The resonance bandwidth is also indicated by curves

$$f_H \pm \frac{\nu}{2\pi}$$

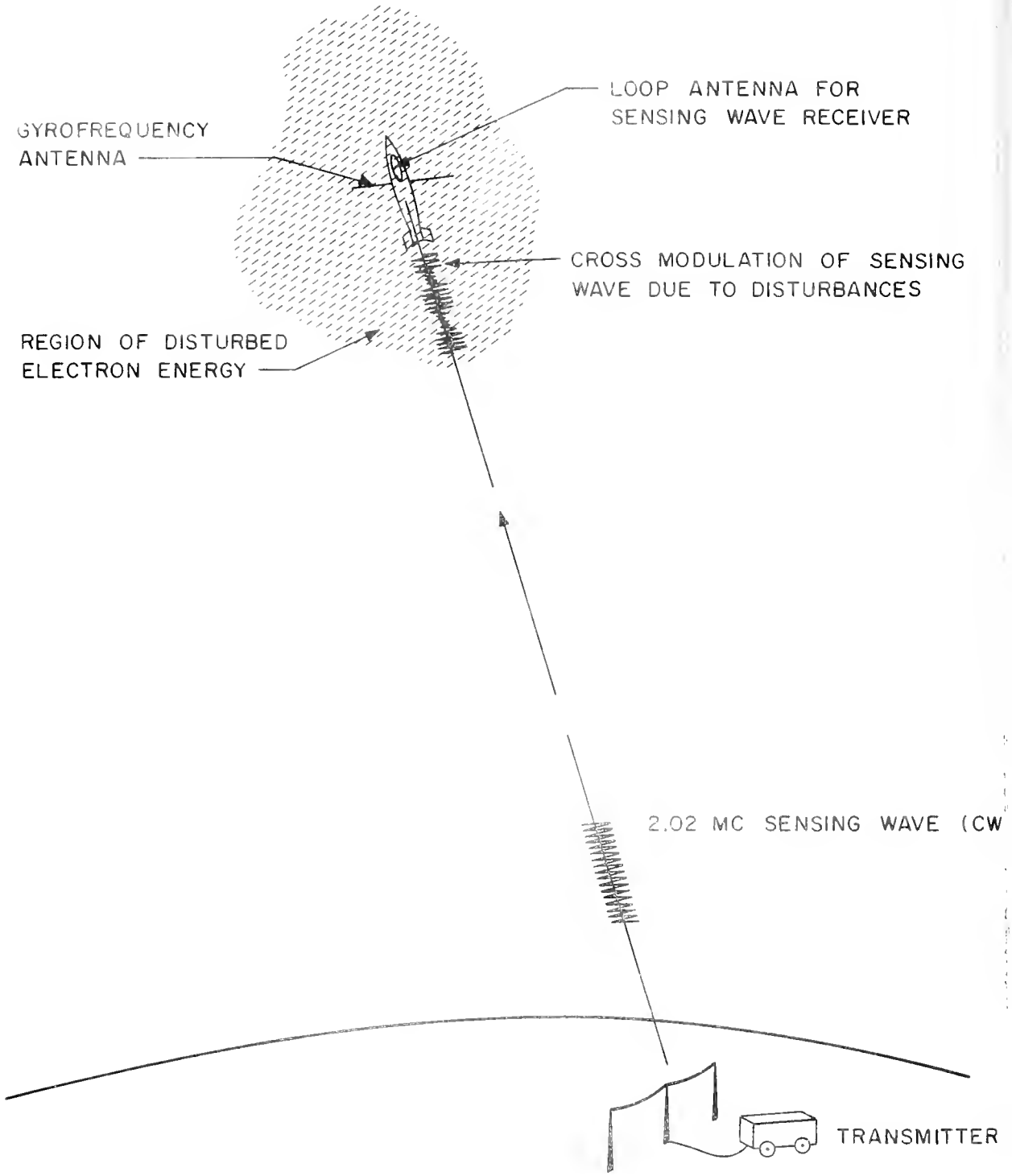

Figure 1. Schematic representation of a gyro-interaction rocket experiment.

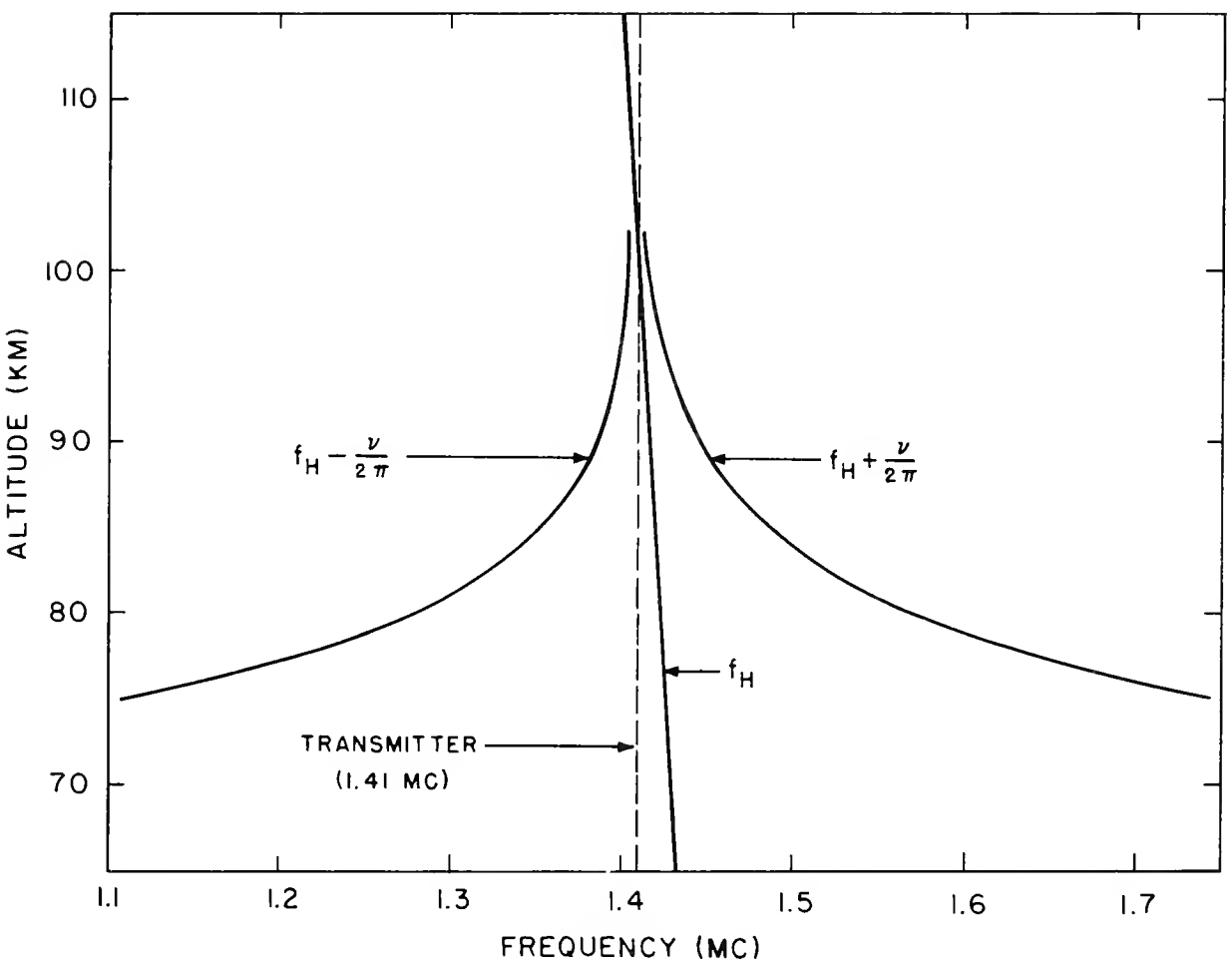

Figure 2. Gyrofrequency f_H and gyroresonance band limits $f_H \pm \nu/2\pi$ as functions of altitude. The frequency of the pulsed gyrofrequency transmitter (1.41 Mc) is indicated as a dashed line.

where the values of collision frequency ν are from reference 5. The frequency used in the experiments is the gyrofrequency at 100 km (i.e., 1.41 Mc). This choice was based on two factors. First, the gyrofrequency at any altitude above 110 km would be outside the resonance near 100 km, as can be seen in Figure 2. Second, the resonance half-width at 100 km corresponds to roughly 0.4% of the gyrofrequency. This is the same order of magnitude as the error which may result from the approximation used in computing the terrestrial magnetic field.[11]

The choice of the sensing wave frequency was the result of consideration of several factors. Cross-modulation by weak gyro-interaction effects (where only increased electron temperature is involved) requires that the absorptive index near the rocket be large and strongly dependent on collision frequency. As the index of absorption is proportional to electron density as well as collision frequency, both are important. It is desirable that the total absorption be great enough to eliminate a strong reflected component of the sensing signal which would produce a standing wave. In addition, the reflection height determines the upper altitude limit of the cross-modulation experiment. The last consideration points to using as high a frequency as is commensurate with the other requirements; the others are best satisfied for lower frequencies. Ideally the frequency would have been chosen on the basis of electron density and absorption measurements made by an ionospheric sounder just prior to each flight. However, the practical considerations of instrumentation and frequency allocation required that the sensing wave frequency be chosen much earlier. To do this a set of absorption versus altitude computations for the ordinary and extraordinary waves propagating parallel with the terrestrial magnetic field was made by Shubert.[12] These were for various

frequencies, both above and below the gyrofrequency, and for several ionospheric models. As might be expected, wave absorption was sensitive to the model. It was indicated that the best choice of frequency would be in the range of 1.8 to 2.5 Mc; the frequency used was 2.02 Mc. The computations also showed that the experiment should be performed in the daytime, near noon, when the D region electron content is maximum. In the first experiment the frequency choice of 2.02 Mc was ideal from the absorption standpoint. In addition its nearness to the gyrofrequency and the consequential anisotropy of the ionosphere resulted in an unexpected form of cross modulation resembling Faraday rotation of the sensing wave at low altitudes. During the second experiment D region electron densities were small, and this frequency did not give optimum results. Further discussion of these observations are included in Section 5.

The Aerospace Launch Facility at Eglin Air Force Base was chosen for these experiments because its location permits rockets to be launched to the south. The propagation of the sensing wave from the launch site to the rocket is nearly parallel with the terrestrial magnetic field. Thus the quasi-longitudinal approximations of magneto-ionic theory are applicable to the sensing wave over much of the rocket trajectories.

5 EXPERIMENTAL RESULTS

Data from a cross-modulation experiment is interpretable only to the extent that the nature of the disturbance of the electron distribution function is known. It is not likely that this could be accurately determined since it would require knowledge of various collisional processes which are not fully understood (i.e. the processes of collisional ionization, detachment, attachment, recombination, and inelastic collisions). A more satisfactory scheme is to determine a plausible model for the disturbance which would produce the observed cross-modulation. This is analogous to attempting to specify a function from a measurement of one of its properties. Obviously the model is not unique. Nevertheless this technique has been employed with some apparent success, as will be shown in this section.

In the first gyro-interaction rocket experiment, GIRE-I, a short dipole was used for the gyrofrequency pulses. A device to step the gyrofrequency transmitter output power through several levels failed early in the flight, resulting in the highest power level being emitted throughout the experiment. The cross-modulation wave shapes indicated that the gyrofrequency fields were so intense as to have caused local increases in electron density, probably due to breakdown or perhaps enhanced collisional detachment, through most of the flight. The interpretation of the cross-modulation gives the attachment rate for free electrons. This is discussed in Section 5.1.

To explore weaker gyro-interaction effects a small loop antenna was used for the disturbing gyrofrequency pulses in the second experiment, GIRE-II. The cross-modulation from this flight gives the rate of loss of excess electron energy. These and other results are included in Section 5.2.

For convenience the notations used in this section are listed here. Frequencies are denoted as:

f = frequency

ω = angular frequency

Physical quantities are designated:

e = electronic charge

m = electron mass

ϵ_o = permittivity of free space

μ_o = permeability of free space

c = velocity of light in free space

k = angular wave number or Boltzmann's constant as indicated

$k_o = \omega/c$

E = RF electric field intensity

H = RF magnetic field intensity

B_o = magnetic induction of the terrestrial field

T = electron temperature

T_o = equilibrium gas temperature

t = time

$\zeta_o = \sqrt{\mu_o/\epsilon_o}$

The plasma parameters are:

N = electron density

$f_N = (Ne^2/4\pi^2 m\epsilon_o)^{1/2}$ = plasma frequency

$f_H = |e B_o/2\pi m|$ = gyrofrequency

ν = collision frequency

ν_o = collision frequency in thermal equilibrium ($T = T_o$)

G = fraction of excess energy lost by an electron per collision

a = electron attachment rate

Dimensionless quantities commonly used in magneto-ionomic theory are given the URSI recommended designations

$$X = (\omega_N/\omega)^2$$

$$Y = \omega_H/\omega$$

$$Z = \nu/\omega$$

$$U = 1 - j\,Z$$

Other quantities and coordinates having only limited usage are assigned notations as required Units are generally MKS rationalized; exceptions are in the presentation of some data which are commonly expressed in CGS units in the literature (e g , electron density is given in cm^{-3} rather than $meter^{-3}$)

5 1 GIRE-I

The initial gyro-interaction rocket experiment, GIRE-I, was instrumented to provide as intense heating of electrons as was practical The gyrofrequency transmitter had a peak available power of 400 w Provision was made to step an attenuator between the transmitter and the dipole antenna through the levels of 0, -10, and -20 db to vary the disturbance. Also included were measurements of the radiated gyrofrequency field, the impedance and radiated power of the gyrofrequency antenna, excitation light and mixing of the gyrofrequency and sensing signals A functional block diagram of the experiment is shown in Figure 3 Locations of the various antennas with respect to the rocket nose cone are shown in Figure 4 Early in the flight, just as sustainer burnout occurred, a motor driven switch, which served as the clock and as a data commutator, failed This resulted in the stoppage of many functions within the payload The gyrofrequency transmitter continued to function in a free-running mode of operation, but the only data obtained were the output and the AGC voltage of the sensing wave receiver All other measurements were lost

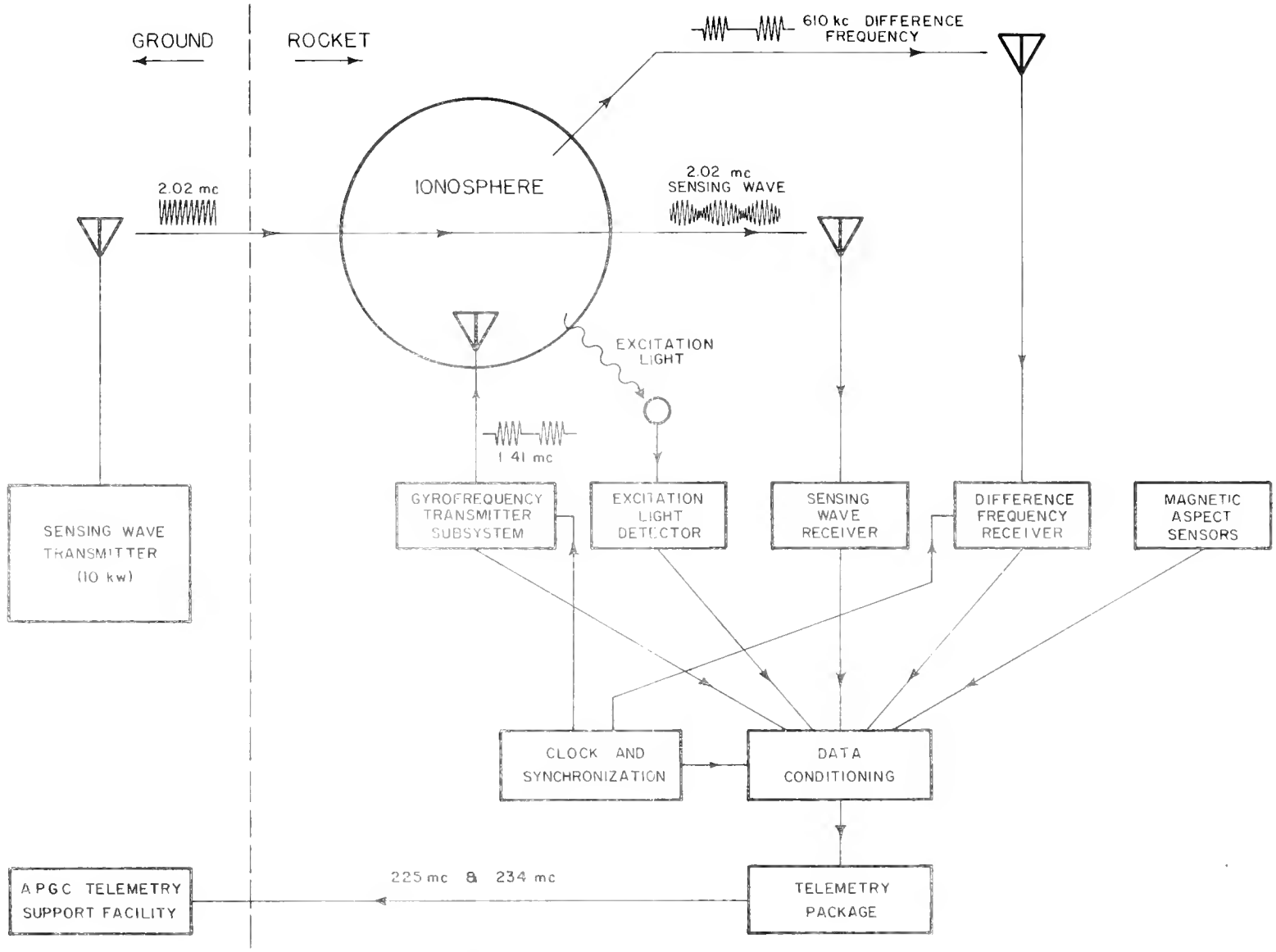

Figure 3. Functional block diagram of GIRE-I.

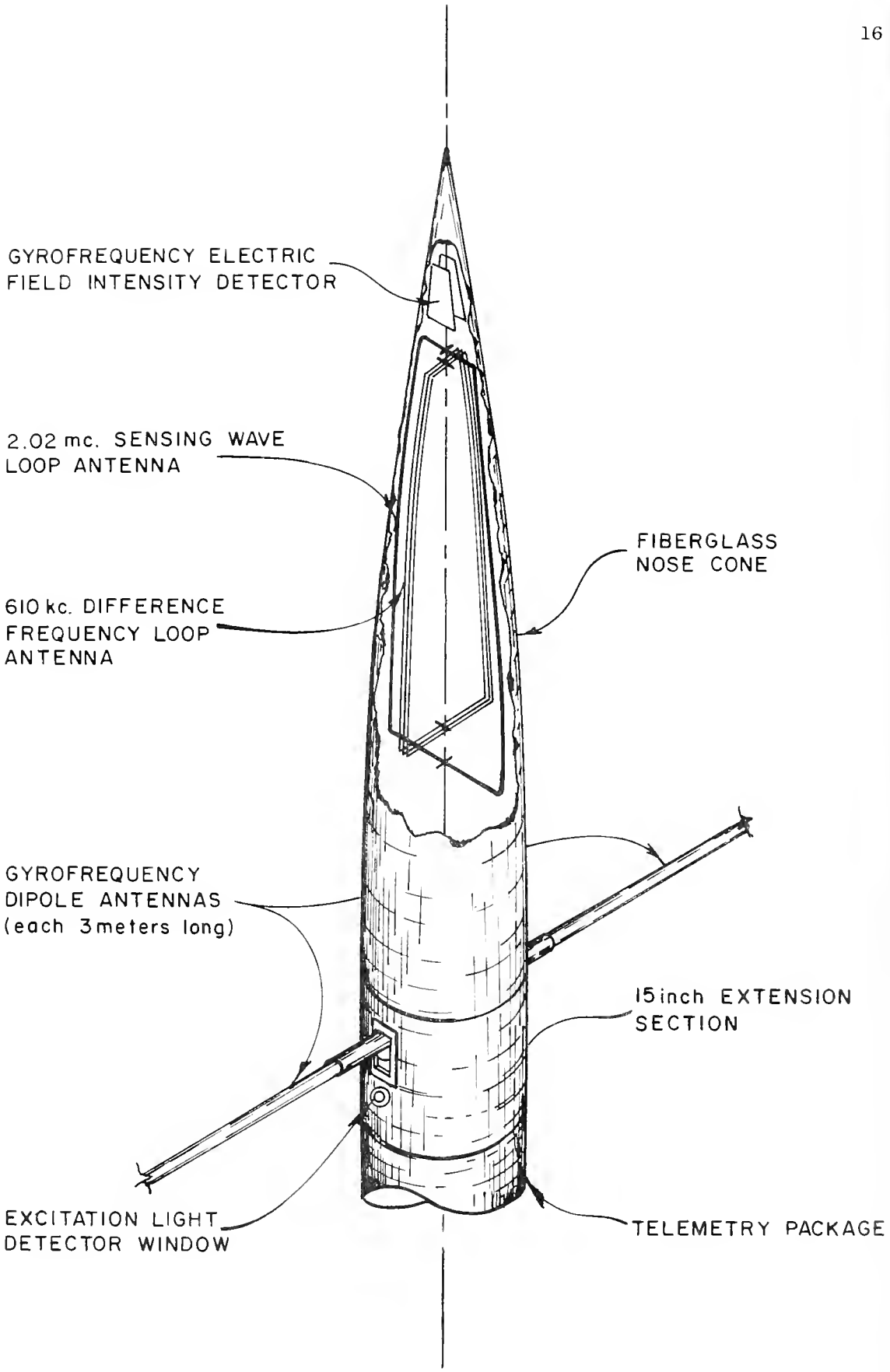

Figure 4. Locations of antennas (GIRE-I).

The instrumentation of this payload was described in reference 13. Only the portions which have bearing on the data will be discussed here.

5.1.1 Flight Information

The GIRE-I payload was carried by an Aerobee AJ10-25 rocket (AFCRL No. AA1.193). The vehicle configuration is shown in Figure 5. Launch took place on 1 May 1962 at 1318 hours CST from the Aerospace Launching Facility at Eglin Air Force Base, Florida. The Aerobee tower from which the vehicle was launched is located at 30^{o} 23' 40.842" north latitude and 86^{o} 42' 59.544" west longitude.

A plot of the trajectory of the rocket computed from radar tracking data is shown in Figure 6. The bearing at impact was 191^{o} true.[14] Since the terrestrial magnetic field in the northern hemisphere dips to the north, the path of the sensing wave to the rocket was nearly parallel with the magnetic field. Thus the quasi-longitudinal approximations of magneto-ionic theory are applicable to the sensing wave over much of the flight.

During the first few seconds after launch while the vehicle was powered by the first stage, or booster, the magnetometer data showed that the rocket spin was clockwise when viewed from the ground. This was confirmed by phototheodolite records. However, under power of the second stage, or sustainer, rotation gradually changed to counterclockwise. Magnetometer data ceased with sustainer burnout and the failure of the commutator at 21 km Nulls of the sensing wave receiver input continued to be regular through this region, indicating that the rotation probably remained counterclockwise.

5.1.2 Gyrofrequency Disturbance Pulses

The clock failure left the gyrofrequency transmitter operating with a pulse repetition time of 22 milliseconds. This was the unsynchronized time determined within the modulator The pulse width was 500 microseconds Peak

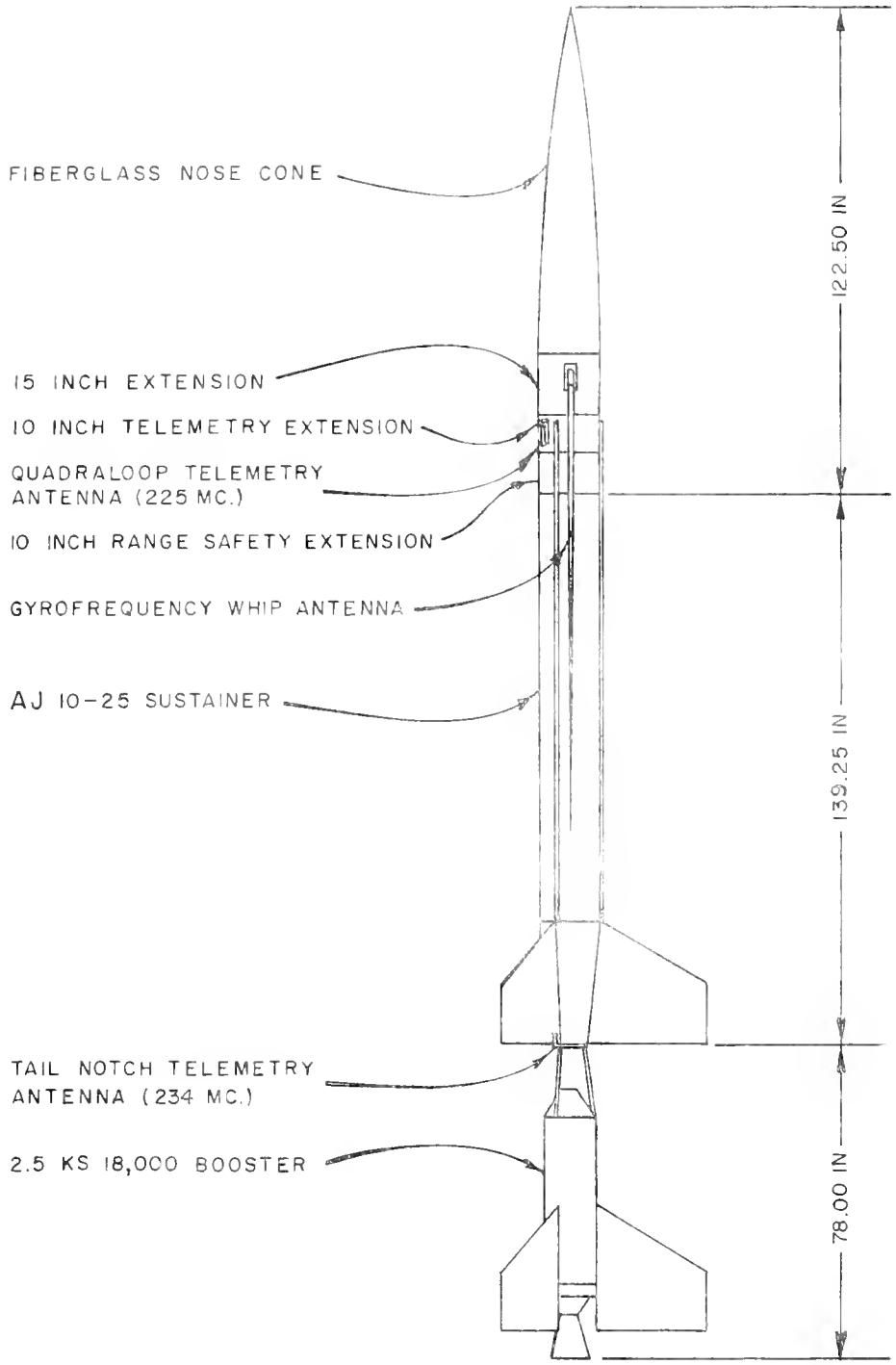

Figure 5. Vehicle configuration for GIRE-I.

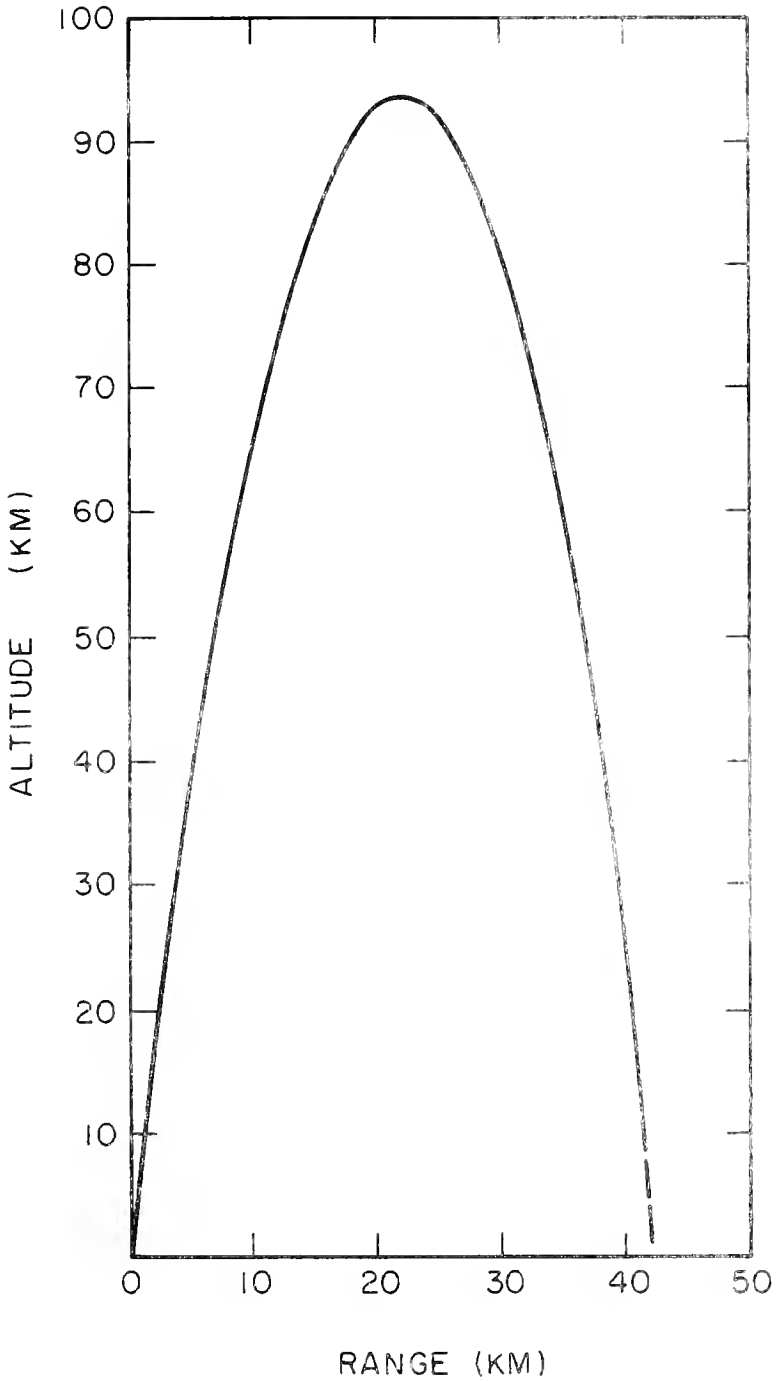

Figure 6. Trajectory of GIRE-I (1318 CST 1 May 1962). The bearing to the point of impact was 191° true.

power available at the antenna was left at 400 watts throughout the unpowered portion of the flight.

The gyrofrequency dipole antenna consisted of two fiberglass whips, each 3 meters long. Initially these were secured along the side of the rocket body. They were to be extended a fixed time after launch as determined by an acceleration actuated timer. The prearranged time corresponded to approximately 63.5 km Confirmation of deployment was not obtained due to the aforementioned failure. However, a change in the cross modulation data at this time indicated that the whips were probably deployed as planned.

5.1.3 Cross-Modulation of Sensing Wave

To minimize the effect of the ionosphere on the performance of the receiving antenna in the rocket a loop was used. As is indicated in Figure 4 it was oriented to be orthogonal to the gyrofrequency antenna to minimize interference. Furthermore rotation of the rocket in ascent would result in periodic nulls in the receiver input if the sensing wave were linearly polarized.

The receiver was constructed by Kellogg Space Communications Laboratory. It was fixed tuned to 2.02 Mc with 10 kc output bandwidth. An output of approximately +10 volts for RF inputs in the range of 1 microvolt to 1 volt was provided. The AGC time constant was greater than 100 milliseconds over this range. An AGC voltage was available for telemetring the field intensity.

Because of linear detection a 1 volt change in the receiver output corresponded to 10% change in the input. A bias of -6.7 volts was added to the output so that the 0 to 5 volt range of the telemetry subcarrier oscillator corresponded to -33% to +17% fluctuations of the input.

Failure of the data commutator left the AGC voltage of the receiver connected directly to a subcarrier oscillator. Thus, fortuitously, the AGC data was obtained.

Sensing wave data shows cross-modulation for all altitudes above 40 km. However, with the deployment of the gyrofrequency dipole antenna at 63.5 km, each disturbance became so intense that the data is uninterpretable past this point.

From 40 km to 63.5 km during ascent a characteristic form of cross-modulation was detected near each null of the sensing wave receiver input. Figure 7 shows the sensing signal near a null at 52.6 km, which is typical of the data in this altitude range. The general shape of the curve is due in part to AGC action. In general this cross modulation began several degrees prior to each null as a periodic decrease in the signal. Near the null it changed to an increase and disappeared several degrees past the null.

These nulls were undoubtedly due to the rotation of the rocket. As the axis of this rotation was probably very nearly in line with the direction of travel of both the rocket and the sensing wave, the form of cross modulation suggests an explanation based on a slight rotation and subsequent relaxation of the plane of polarization of the sensing wave with each gyrofrequency pulse. To illustrate this conjecture it is convenient to use the spinning rocket as a reference, in which case the plane of polarization of the sensing wave rotates with rate ω_r about the rocket. The normal receiver input V_i can then be expressed as

$$V_i = V_s \left| \sin \omega_r t \right| \qquad (5.1)$$

A perturbation of the plane of polarization by the angle δ would result in

$$V_i(\delta) = V_s \left| \sin(\omega_r t - \delta) \right| \qquad (5.2)$$

These functions are sketched for a period of one-half revolution of the rocket

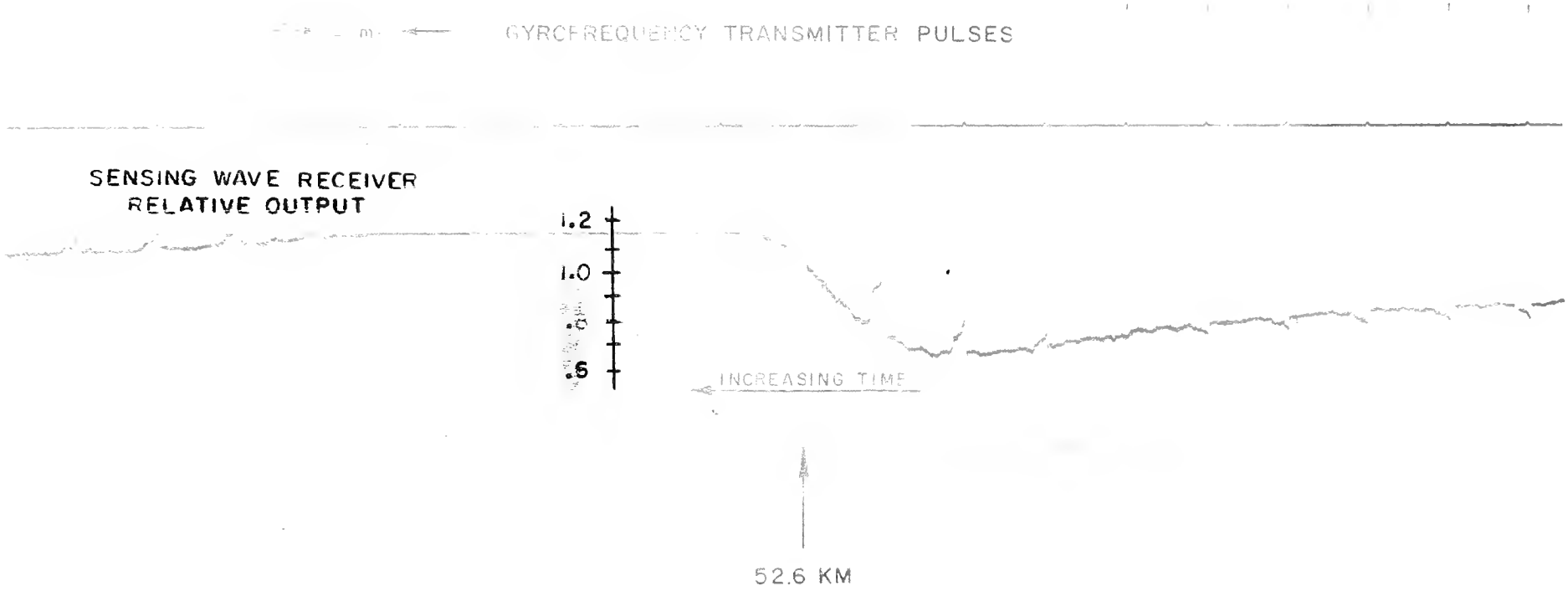

Figure 7. Characteristic modulation of sensing wave near polarization null at 52.6 km. (GIRE-I) Rocket Velocity = 900 meters/second; Rotation Rate = 42.2°/second.

with $\delta = -3^{o}$ in Figure 8a. If the cross-modulation were due only to a switching of the plane of polarization between $\omega_r t$ and $(\omega_r t - \delta)$ the modulation would be the difference in these two curves. It can be seen that this difference is initially negative but changes to positive just prior to the null at $\omega_r t = \delta/2$. A more meaningful quantity is the modulation envelope which would appear at the receiver output under ideal AGC conditions. Ideally the gain of the receiver g should be controlled so that the normal receiver output V_o is independent of time, or

$$g = \frac{V_o}{V_i} \tag{5.3}$$

Under perturbed conditions the output $V_o(\delta)$ would be

$$V_o(\delta) = V_o \left(\frac{V_i(\delta)}{V_i} \right) \tag{5.4}$$

The latter expression is the envelope of cross modulation which would occur. This is shown graphically in Figure 8b. The similarity of the curve $V_o(\delta)$ with the envelope of the cross-modulation of Figure 7 is fairly close.

A first assumption regarding the mechanism of the apparent wave rotation indicated in the data would logically be one based on Faraday rotation. This occurs for waves traveling nearly parallel with the terrestrial magnetic field because of the difference in phase velocity of the two characteristic waves. A slight modification of collision frequency or electron density, or both, along a portion of the sensing wave path would change the difference in phase velocities of the waves and hence produce a slight rotation of the wave from its normal condition. A closer observation of Figure 7 shows that the effect of each gyrofrequency disturbance persisted about 5 milliseconds, after which the cross-modulation ended very abruptly. Were the process purely collisional,

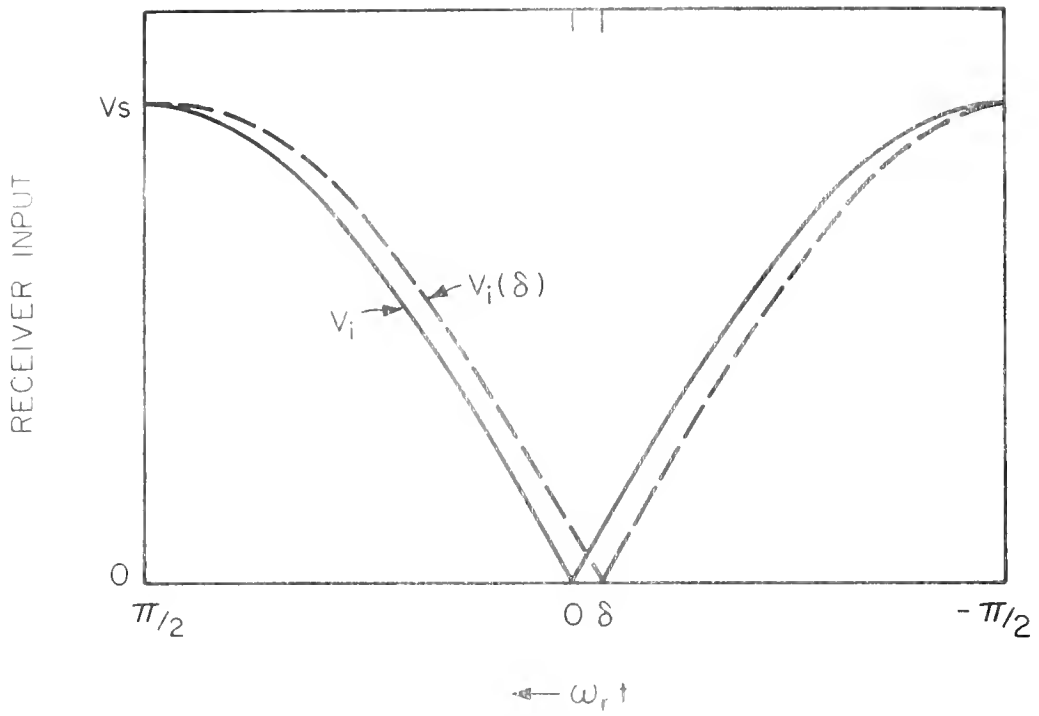

Figure 8a. Normal receiver input V_i and perturbed input $V_i(\delta)$ as functions of $\omega_r t$ for $\delta = -3^o$.

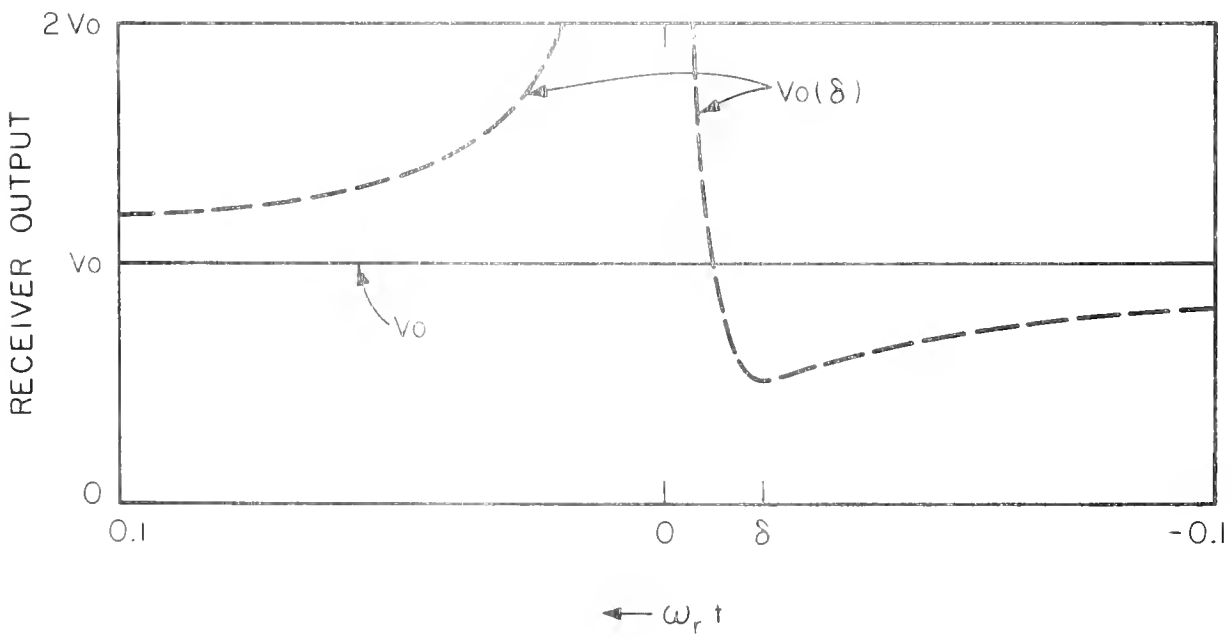

Figure 8b. Normal receiver output V_o and perturbed output $V_o(\delta)$ near a null of V_i for $\delta = -1^o$.

the energy decay would have required much less than one millisecond A second possibility is that electron density was increased with each gyrofrequency pulse, but removal of the excess electrons would have required much longer than 5 milliseconds. These factors lead to the conjecture that each disturbance was relatively small and consisted of a bubble-like region of excess electrons. At the end of each gyrofrequency pulse the rocket was near the center of such a bubble. Electron temperature, greatly increased during the gyrofrequency pulse, would return to equilibrium in a short time, accounting in part for the transient at the start of each cross-modulation waveform. After this the rate of change of the receiver input would be determined by the rate of loss of excess electrons due to attachment. As the rocket progressed out of the bubble, the cross-modulation would terminate.

This explanation is of course not compatible with the usual concept of Faraday rotation. The latter would require that each disturbance be uniform and spread over a large region (in terms of wavelengths) However, subsequent analysis will show that an effect equivalent to wave rotation can be produced on the sensing wave. This is due to the anisotropic properties of the medium and will occur even if only a small bubble-like region of excess electrons surrounding the antenna is produced

To show that this conjecture is plausible it is convenient to establish a model to represent the physical relationships of the sensing wave, the receiving loop antenna (in the rocket), and the disturbance (of excess electrons). In the ascent portion of the flight the path of the sensing wave to the rocket and the direction of travel of the rocket were very nearly parallel with the terrestrial magnetic field B_o The z coordinate direction will be oriented to coincide with the magnetic field As B_o is downward in the

northern hemisphere, the propagation vector of the sensing wave k and the motion of the rocket are assumed to be in the -z direction. In Figure 9a these relationships are shown. The sensing wave coordinates are (x,y,z) while those of the rocket are (x', y', z). The components of the sensing wave (designated by the subscript A) incident on the rocket are assumed to be

$$E_A = \hat{x}\, e^{j k_o z}$$
$$H_A = -\hat{y}\, \frac{1}{\zeta_o}\, e^{j k_o z} \qquad (5.5)$$

This presumes that the equilibrium electron density in the region of interest (i.e., below 65 km) has negligible effect on the sensing wave, and hence the wave number is k_o.

Rotation of the rocket in the GIPE-I flight was such as to increase with time the angle ϕ between the x and x' axes as indicated in Figure 9b. This sketch also shows the orientation of the receiving loop antenna in the x'z plane and the coordinate system (r, θ, ϕ') to be used in describing the fields of the loop and the distribution of excess electrons in the disturbance.

The output of the sensing wave receiver V is related to the sensing wave field A by the expression

$$V = g \left| \langle A \,\mathscr{J}\, B \rangle \right| \qquad (5.6)$$

where g is proportional to the receiver gain and $\langle A \mathscr{J} B \rangle$ is the reaction of the sensing wave transmitting antenna $\langle A$ with the receiving loop antenna $B \rangle$. The propagator for the medium is $\mathscr{J}$ (see reference 15 for the notation). For the case in question the medium may be considered to be free space except for

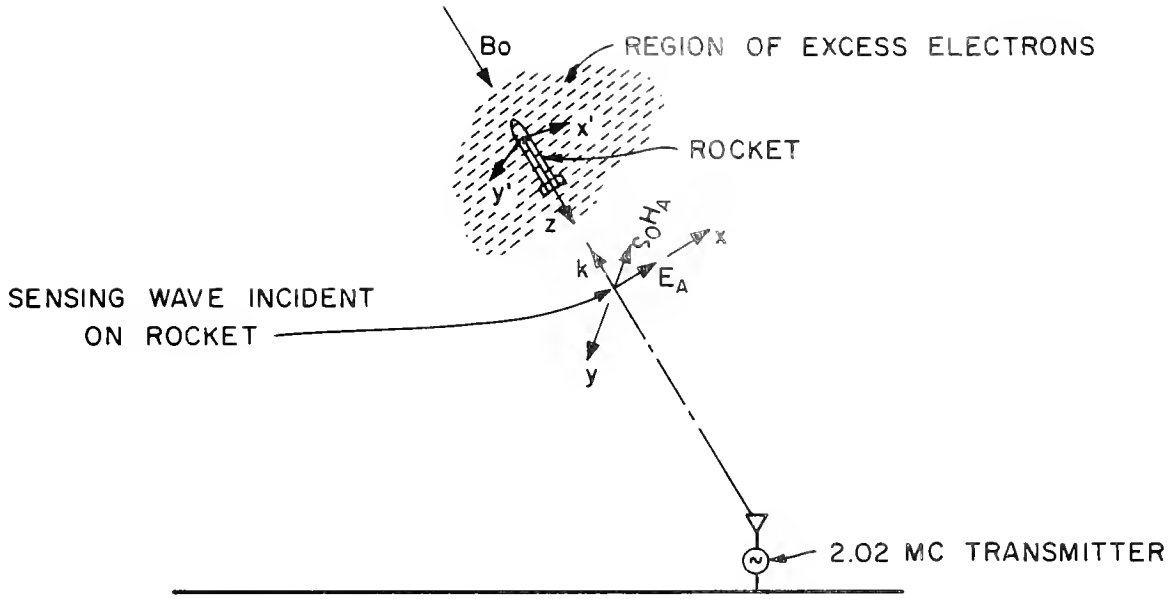

Figure 9a. Assumed relationships between the sensing wave, rocket and B_o.

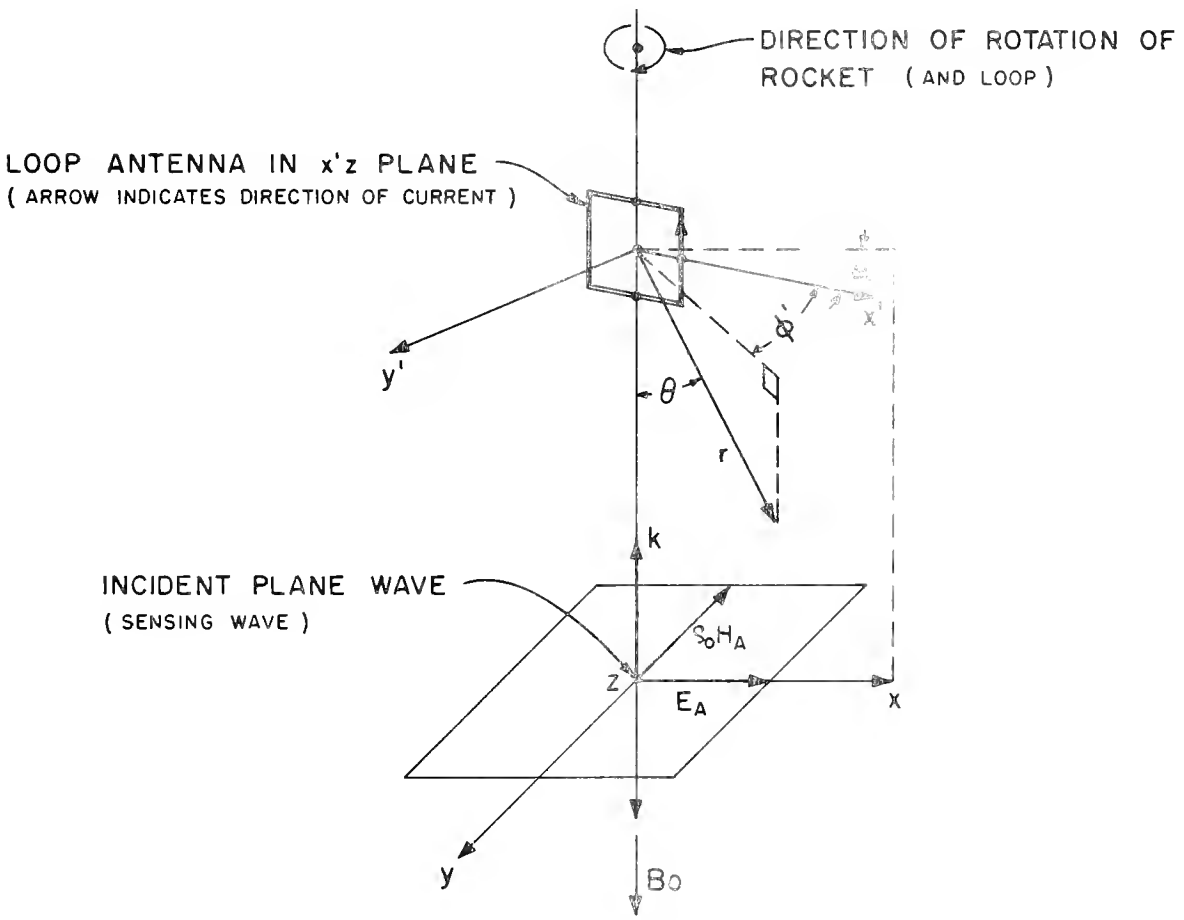

Figure 9b. Relationships between the sensing wave and rocket coordinate systems.

the small disturbed region surrounding the rocket, in which there are excess electrons. The Born approximation is particularly suited to this problem, from which

$$\langle A \mathcal{G} B \rangle \cong \langle A \mathcal{G}_o B \rangle + \langle A \mathcal{G}_o M \mathcal{G}_o B \rangle \qquad (5.7)$$

where $\mathcal{G}_o$ is the propagator for free space and M represents the conductivity within the disturbance. The first term of Equation (5.7) is the free space reaction and is just the integral of the sensing wave field $\langle A \mathcal{G}_o$ over the loop current distribution $B\rangle$. In the second term $\langle A \mathcal{G}_o M$ may be considered as a secondary source of induced currents in the region of excess electrons. Thus the disturbance contributes the reaction of a secondary, or induced, source $\langle A \mathcal{G}_o M$ with the loop current distribution $B\rangle$.

The free space part of Equation (5.7) may be found most conveniently by first replacing the loop with an equivalent magnetic dipole. For unit current in the loop circulating in the direction indicated in Figure 9b the equivalent magnetic source of length L has current[16]

$$K_B = \hat{y}' \, j \frac{\omega \mu_o S}{L} \qquad (5.8)$$

where S is the area enclosed by the loop. With the use of this current distribution for $B\rangle$ the free space part of Equation (5.7) is

$$\langle A \mathcal{G}_o B \rangle = -\int_{-L/2}^{L/2} dy' \, H_A \cdot K_B = j \, k_o \, S \cos \phi \qquad (5.9)$$

This shows the expected result that the response of the antenna depends upon the cosine of the angle between the sensing wave electric field vector and the plane of the loop.

To find the contribution of the disturbance to Equation (5.7) it is first necessary to make assumptions regarding the disturbance. If electrons were generated by a collisional process during a gyrofrequency pulse, the mean electron energy at the end of the pulse would have been rather high. The time required for the electron temperature to reach equilibrium with the gas molecules is determined by the time constant $(G\nu)^{-1}$ sec. At 65 km Fejer and Vice[5] give $\nu \cong 10^7$. It is generally acceptable that $G > 10^{-3}$ for air, in which case $(G\nu)^{-1} < 10^{-4}$ sec below 65 km. Therefore thermal equilibrium should have been established in less than a millisecond following each gyrofrequency pulse. The duration of the cross modulation for several milliseconds is attributed to a small region of excess electrons in thermal equilibrium with the gas molecules.

Since the disturbance is assumed to involve only electrons, the conductivity represented by M in Equation (5.7) is just the conductivity tensor σ. For a magnetoplasma with B_o in the z direction

$$\sigma = \begin{vmatrix} \sigma_{xx} & \sigma_{xy} & 0 \\ \sigma_{yx} & \sigma_{yy} & 0 \\ 0 & 0 & \sigma_{zz} \end{vmatrix} \tag{5.10}$$

When the Appelton-Hartree approximation is used, the various entries are

$$\sigma_{xx} = \sigma_{yy} = -j\omega\epsilon_o \frac{XU}{U^2 - Y^2} \tag{5.11}$$

$$\sigma_{xy} = \sigma_{yx} = \omega\epsilon_o \frac{XY}{U^2 - Y^2} \tag{5.12}$$

$$\sigma_{zz} = -j\omega\epsilon_o \frac{X}{U} \tag{5.13}$$

All terms of σ are proportional to X and hence to electron density N. Therefore the conductivity can be expressed as

$$\sigma = N \sigma' \tag{5.14}$$

where the matrix σ' can be identified as e times the electron mobility. This form is convenient because N is assumed to be a function of position (r, θ, ϕ') and time t while σ' is independent of these.

Because of the form of the conductivity tensor, Equation (5.10), the induced electric current density in the disturbance due to the sensing wave field, Equation (5.5), is

$$\langle A \mathscr{J}_o M = (\hat{x}\, \sigma'_{xx} + \hat{y}\, \sigma'_{yx})\, N\, e^{j k_o z} \tag{5.15}$$

Note that the induced current includes a component in the $\hat{y}$ direction because of the gyrotropic property of σ. This is the component responsible for the apparent wave rotation which was observed in the GIRE-I experiment.

With unit current input the free space electric field of the assumed loop is[16]

$$E_B = \hat{y}' \wedge \hat{r}\, \frac{\zeta_o S k_o^3}{4\pi}\, e^{-j\tau} \left(\frac{1}{\tau} - j \frac{1}{\tau^2} \right) \tag{5.16}$$

where $\tau = k_o r$. The second term of Equation (5.7) thus becomes

$$\langle A \mathscr{J}_o M \mathscr{L}_o B \rangle = \int d^3\tau\, (\sigma_{xx}'\, \hat{x} \wedge \hat{y}' + \sigma_{yx}'\, \hat{y} \wedge \hat{y}')$$

$$\cdot\, \hat{r}\, e^{j\tau \cos\theta}\, N \mathscr{E}_B \tag{5.17}$$

where $\mathcal{E}_B$ is the amplitude of E_B. Evaluation of the vector operations gives

$$\langle A \mathcal{G}_o M \mathcal{J}_o B \rangle = \zeta_o S (\sigma'_{xx} \cos \phi - \sigma'_{yx} \sin \phi) I \tag{5.18}$$

where

$$I = \frac{1}{4\pi} \int_o^\infty d\tau \, e^{-j\tau}(\tau - j) \int_o^\pi d\theta \sin\theta\cos\theta \, e^{j\tau \cos\theta} \int_o^{2\pi} d\phi' N(\tau, \theta, \phi', t) \tag{5.19}$$

It should be noted that the integral I does not depend on the angle of rotation of the rocket with respect to the sensing wave, and thus I is a characteristic of the disturbance $N(\tau, \theta, \phi', t)$. It can also be seen that the dependence of N on ϕ' is unimportant to the evaluation of I. Thus

$$I = \frac{1}{2} \int_o^\infty d\tau \, e^{-j\tau} (\tau - j) \int_o^\pi d\theta \sin\theta\cos\theta \, e^{j\tau\cos\theta} \mathcal{N}(\tau, \theta, t) \tag{5.20}$$

where $\mathcal{N}(\tau, \theta, t)$ is an effective electron density distribution. It is the average about the z axis of the actual distribution, i.e.,

$$\mathcal{N}(\tau, \theta, t) = \frac{1}{2\pi} \int_o^{2\pi} d\phi' N(\tau, \theta, \phi', t) \tag{5.21}$$

The integral I will be discussed later for various forms of the distribution N.

Combining Equations (5.9) and (5.18) gives the complete Born approximation for the reaction:

$$\langle A \mathcal{J} B \rangle = j k_o S \left[\left(1 - j I \frac{\sigma'_{xx}}{\omega \epsilon_o} \right) \cos \phi - j I \frac{\sigma'_{yx}}{\omega \epsilon_o} \sin \phi \right] \tag{5.22}$$

The receiver output is then

$$V = g \left| \left(1 - j\, I \frac{\sigma'_{xx}}{\omega \epsilon_o}\right) \cos \phi - j\, I \frac{\sigma'_{yx}}{\omega \epsilon_o} \sin \phi \right| \qquad (5.23)$$

Under normal, or undisturbed, conditions $I = 0$; in a region of excess electrons I is non-zero and produces cross-modulation.

The characteristic cross-modulation from the GIRE-I data (cf. Figure 7) was essentially antisymmetric about each null. Prior to the null cross-modulation decreased the receiver output; after the null it was increased. These nulls correspond to $\phi = \pi/2$ in Equation (5.23). A similar antisymmetric behavior is exhibited by Equation (5.23) when the coefficient of $\sin \phi$ has the property

$$\mathrm{Re}\left[j\, I \frac{\sigma'_{yx}}{\omega \epsilon_o} \right] > 0 \qquad (5.24)$$

during the time I is non-zero (i.e., while the rocket is in the disturbance). The remaining contribution of I to Equation (5.23) is to produce a symmetric component of cross-modulation about $\phi = \pi/2$. In particular the imaginary part of the coefficient of $\sin \phi$ produces an increase in the receiver output symmetric about the null. This could explain the observation that cross-modulation prior to the null was smaller than that after the null, as can be seen in Figure 7.

It is now necessary to explore the conditions for which the bubble-like model of the disturbance can give the observed receiver output, i.e., for which condition (5.24) is satisfied. As a matter of convenience the conductivity given by the Appelton-Hartree formula will be used. The accuracy of this formula, which neglects the dependence of collision frequency on electron

energy, is suspect.[17] Therefore the results will be treated only qualitatively where collision frequency is a factor. From Equation (5.12) and the definitions of $X \left(= \frac{N e^2}{m \epsilon_o \omega^2} \right)$ and $U \left(= 1 - jZ \right)$

$$j I \frac{\sigma'_{yx}}{\omega \epsilon_o} = \frac{I Y e^2}{m \omega^2} \left[\frac{2Z + j(Z^2 + Y^2 - 1)}{(Z^2 + Y^2 - 1)^2 + 4Z^2} \right] \tag{5.25}$$

Thus condition (5.24) can be reduced to the condition

$$2 Z \, \mathrm{Re}\, I - (Z^2 + Y^2 - 1) \, \mathrm{Im}\, I > 0 \tag{5.26}$$

The value of Z is some effective value which is probably the order of unity or greater below 65 km. Since $Y^2 \cong 0.5$ for the sensing wave frequency it can be assumed that

$$\left(Z^2 + Y^2 - 1 \right) > 0 \tag{5.27}$$

below 65 km.

The next step is the evaluation of the integral I, Equation (5.19). An arbitrary distribution of electrons in some bounded region $r < k_o R$ may be expanded as a sum of orthogonal density functions such as

$$N(r, \theta, \phi') = \begin{cases} \sum_{n=0}^{\infty} \sum_{s=1}^{\infty} N_{ns} P_n^o (\cos \Theta) \mathcal{J}_c (s\beta r) \\ + \sum_{m=1}^{n} \sum_{n=1}^{\infty} \sum_{s=1}^{\infty} (N^{\epsilon}_{mns} \cos m\phi + N^{o}_{mns} \sin m\phi') P_n^m (\cos \Theta) \, {}_o(s\beta r) \\ \qquad\qquad\qquad\qquad\qquad\qquad \left[\text{for } r < k_o R \right] \\ 0 \qquad\qquad\qquad\qquad\qquad\qquad \left[\text{for } r > k_o R \right] \end{cases} \tag{5.28}$$

where the $P_n^m(\cos \Theta)$ are Legendre functions and $\mathcal{J}_o(s\beta r)$ are zero order spherical Bessel functions, i e

$$\mathcal{J}_o(s\beta r) = \frac{\sin s\beta r}{s\beta r} \tag{5.29}$$

The coefficient β is defined by

$$\beta = \frac{\pi}{k_o R} \tag{5.30}$$

so that the functions $\mathcal{J}_o(s\beta\tau)$ vanish at $\tau = k_o R$ for all s.

As given by Equation (5.21) the effective electron density $\mathcal{N}(\tau,\theta)$ of the disturbance described by Equation (5.28) is just

$$\mathcal{N}(\tau,\theta) = \sum_{n=o}^{\infty} \sum_{s=1}^{\infty} N_{ns} P_n^o(\cos\theta) \mathcal{J}_o(s\beta\tau) \tag{5.31}$$

The integral I, Equation (5.20), is then

$$I = \sum_{n=0}^{\infty} \sum_{s=1}^{\infty} N_{ns} \mathcal{I}_{ns} \tag{5.32}$$

where

$$\mathcal{I}_{ns} = \frac{1}{2} \int_o^{k_o R} d\tau\, e^{-j\tau}(\tau - j)\mathcal{J}_o(s\beta\tau) \int_o^{\pi} d\theta \sin\theta\cos\theta\, e^{j\cos\theta} P_n^o(\cos\theta) \tag{5.33}$$

The part of $\mathcal{I}_{ns}$ integrated with respect to θ will be designated Θ_n; it has the form

$$\Theta_n = \int_o^{\pi} d\theta \sin\theta \cos\theta\, e^{j\tau\cos\theta} P_n^o(\cos\theta) = -j\frac{d}{d\tau}\int_{-1}^{1} du\, e^{j\tau u} P_n^o(u) \tag{5.34}$$

where $u = \cos\theta$ The last integral of Equation (5.34) is a well-known definite integral, from which

$$\Theta_n = 2(j)^{n-1} \frac{d}{d\tau} \mathcal{J}_n(\tau) \tag{5.35}$$

where $\mathcal{J}_n(\tau)$ is the n-th order spherical Bessel function of τ. Thus

$$\mathcal{I}_{ns} = (j)^{n-1} \int_0^{k_o R} d\tau \, e^{-j\tau}(\tau - j) \, \mathcal{J}_o(s\beta\tau) \, \frac{d}{d\tau} \mathcal{J}_n(\tau) \tag{5.36}$$

It can be seen in Figure 7 that the rocket remained within each disturbance several milliseconds. With a rocket velocity of approximately 1000 meters per second it is evident that the extent of each disturbance was probably less than 4 meters. At 2.02 Mc the wavelength is roughly 150 meters. Therefore the maximum angular dimension of the assumed disturbance may be considered to be small, or

$$k_o R \ll 1 \tag{5.37}$$

Since $k_o R$ is the limit on the integral (5.36) the functions $\mathcal{J}_n(\tau)$ may take on asymptotic values

$$\mathcal{J}_n(\tau) \cong \frac{\tau^n}{1 \cdot 3 \cdot 5 \cdots (2n+1)} \tag{5.38}$$

and therefore

$$\frac{d}{d\tau} \mathcal{J}_n(\tau) \cong \frac{n \, \tau^{n-1}}{1 \cdot 3 \cdot 5 \cdots (2n+1)} \quad [n \geq 1] \tag{5.39}$$

It may be noted that since

$$\frac{d}{d\tau} \mathcal{J}_o(\tau) = -\mathcal{J}_1(\tau) \tag{5.40}$$

then

$$\frac{d}{d\tau} \mathcal{J}_o(\tau) \cong -\frac{5}{2} \mathcal{J}_2(\tau) \tag{5.41}$$

Because of the form of $\mathcal{I}_{ns}$, in Equation (5.36),

$$\mathcal{I}_{os} \simeq \frac{5}{2}\,\mathcal{I}_{2s} \tag{5.42}$$

It is therefore necessary to evaluate $\mathcal{I}_{ns}$ for $n \geq 1$ only. Using the above approximations

$$\mathcal{I}_{ns} = \frac{(j)^{n-1}\, n}{s\beta[1\cdot 2\cdot 3\cdots(2n+1)]} \int_0^{k_o R} d\tau\, e^{-j\tau}\,(\tau^{n-1} - j\tau^{n-2}) \sin s\beta\tau \quad [n \geq 1] \tag{5.43}$$

Neglecting higher order terms in $k_o R$ the first four values of I_{ns} are

$$\mathcal{I}_{os} \simeq \begin{cases} \dfrac{2\left(k_o R\right)^2}{3\left(s\pi\right)^2} & [s \text{ odd}] \\ -\dfrac{\left(k_o R\right)^4}{6\left(s\pi\right)^2} & [s \text{ even}] \end{cases} \tag{5.44}$$

$$\mathcal{I}_{1s} \simeq -j\left(\frac{k_o R}{6s}\right) \tag{5.45}$$

$$\mathcal{I}_{2s} \simeq \begin{cases} \dfrac{4\left(k_o R\right)^2}{15\left(s\pi\right)^2} & [s \text{ odd}] \\ -\dfrac{\left(k_o R\right)^4}{15\left(s\pi\right)^2} & [s \text{ even}] \end{cases} \tag{5.46}$$

$$\mathcal{I}_{3s} \simeq -j\,(-1)^s\,\frac{\left(k_o R\right)^3}{35\left(s\pi\right)^2} \tag{5.47}$$

Other terms may be found from the relation

$$\mathcal{I}_{ns} \cong \frac{n}{s\beta[1\cdot3\cdot5\cdots(2n+1)]}\left\{[1-(-1^s)e^{-jk_oR}](n-2)!\, f_1(s\beta,n) - (-1)^s e^{-jk_oR}\left[\frac{(jk_oR)^{n-1}}{s\beta} + (n-2)!\sum_{q=1}^{n-2}\frac{(jk_oR)^q}{q!} f_2(s\beta,n-q)\right]\right\}$$

$$[\text{for } n > 1] \qquad (5.48)$$

where

$$f_1(s\beta,n) = \begin{cases} (s\beta)^{1-n} & [n \text{ even}] \\ -\frac{2}{3}\, n\,(n^2-1)(s\beta)^{-(n+2)} & [n \text{ odd}] \end{cases} \qquad (5.49)$$

$$f_2(s\beta,n-q) = \begin{cases} (s\beta)^{1+q-n} & [(n-q) \text{ even}] \\ 2q(s\beta)^{q-n} & [(n-q) \text{ odd}] \end{cases} \qquad (5.50)$$

Since electron density is a positive quantity, it is necessary that the dominant isotropic coefficient N_{01} be positive. As can be seen in Equation (5.44), the corresponding integral $\mathcal{I}_{01}$ is real and positive. Therefore the product $N_{01}\mathcal{I}_{01}$ is real and positive and thus contributes to the receiver output the proper sense of cross-modulation; i.e., this part of I, given by Equation (5.32), satisfies condition (5.26). Other terms of I may or may not individually satisfy condition (5.26); each would of course depend on the sign of the product $N_{ns}\mathcal{I}_{ns}$. Further comment on the net result of all terms necessitates a less general assumption regarding the distribution of excess electrons.

The actual electron density distributions produced by the GIRE-I gyrofrequency pulses are of course unknown. It is known that the whip antennas were not extended but rather were secured along the sides of the rocket during the time the cross-modulation in question was detected. For the lack of

better knowledge it will be assumed that each disturbance can be approximated by a bubble of radius R in which all negative ions have been destroyed by collisional detachment and where the electron density is given by

$$N \quad \eta = \begin{cases} N_o e^{-at} & r < R \\ 0 & r \geq R \end{cases} \qquad (5\ 51)$$

where R is small compared with a wavelength, and a is the rate of electron attachment For a symmetrical disturbance motion of the rocket near the center of the bubble would contribute negligibly to the amplitude of cross-modulation Therefore only the cross-modulation with the rocket at z 0 will be considered in this discussion

Substitution of the assumed electron density distribution, Equation (5 51) into Equation (5 20) gives

$$I(t) = \frac{N_o e^{-at}}{2} \int_0^{k_o R} d\tau\ e^{-J\tau(\tau - J)} \int_0^{2\pi} d\theta\ \sin\theta \cos\theta\ e^{J\tau\cos\theta} \qquad (5\ 52)$$

Performing this integration and expanding the result as a series in $k_o R$ results in

$$I(t) = \frac{1}{6} N_o e^{-at} (k_o R)^2 + O(k_o R)^5 \qquad (5\ 53)$$

Since the disturbance is presumed small with respect to a wavelength

$$(k_o R) \ll 1 \qquad (5\ 54)$$

and hence

$$I(t) \sim \frac{1}{6} N_o e^{-at} (k_o R)^2 \qquad (5\ 55)$$

This quantity is real and positive and therefore satisfies condition (5.26). Thus a disturbance given by (5.51) could have produced the form of cross-modulation observed on the GIRE-I sensing wave receiver output.

The receiver output, Equation (5.23), for this case can be expressed

$$V = g \left| (1 - h_1 e^{-at}) \cos \phi - h_2 e^{-at} \sin \phi \right| \tag{5.56}$$

where

$$h_1 = j \frac{N_o (k_o R)^2 \sigma'_{xx}}{6\omega\epsilon_o} \tag{5.57}$$

$$h_2 = j \frac{N_o (k_o R)^2 \sigma'_{yx}}{6\omega\epsilon_o} \tag{5.58}$$

After the brief period during which electron temperature returns to equilibrium with the gas molecules following each gyrofrequency pulse, h_1 and h_2 become constants. Letting the subscript (-) refer to the value of a quantity just prior to a gyrofrequency pulse and (+) to its value just after the electrons reach thermal equilibrium following a pulse, the rate of change of V at $t=t_-$ is given approximately by

$$\left(\frac{dV}{dt}\right)_{t_-} \cong -a (V_+ - V_-) - \left(\frac{dV}{dt}\right)_{t_-} \tag{5.59}$$

This assumes that the rate of change of receiver gain g (due to AGC) is constant in the interval $t_- \leq t \leq t_+$. Solving Equation (5.59) for the attachment rate a gives

$$a \cong \frac{\left(\frac{dV}{dt}\right)_{t_-} - \left(\frac{dV}{dt}\right)_{t_-}}{V_+ - V_-} \tag{5.60}$$

The various quantities in this expression may be obtained from the cross-modulation data

Values of the attachment rate λ obtained from GIRE-1 data by use of Equation (5.60) have been plotted in Figure 10. Error flags indicate the variance of the data near each sensing wave null. It is interesting to note that these values of λ are approximately proportional to corresponding molecular densities given by Minzner et al[18]. This suggests electron removal by a two-body process such as

$$O_2 + e \longrightarrow O_2^- + \text{photon} \qquad (5.61)$$

However the attachment coefficient for such a process would have to be $2 \pm 5 \times 10^{-14}$ cm^3 sec^{-1} which is at least an order of magnitude too large.[19]

A quantity which is greatly affected by the attachment rate is the ratio of negative ion density N_- to electron density N. This is usually designated by λ and is given by

$$\lambda = \frac{N_-}{N} = \frac{\lambda}{d} \qquad (5.62)$$

where d is the coefficient of detachment of electrons from negative ions. Nicolet and Aikin[20] have computed λ for various altitudes, assuming that three-body attachment to molecular oxygen is the dominant removal process. Using a photodetachment rate of $d = 0.44$ sec^{-1} derived from the work of Burch, Smith, and Branscomb,[21] Nicolet and Aikin obtain $\lambda = 7.5$ at 60 km. Assuming the same value of d but using the λ from the GIRE-1 data, a value of $\lambda = 84$ at 60 km is obtained. Recently Bourdeau et al[22] have summarized various measurements, including those of ion densities from several workers.[23-25] There is

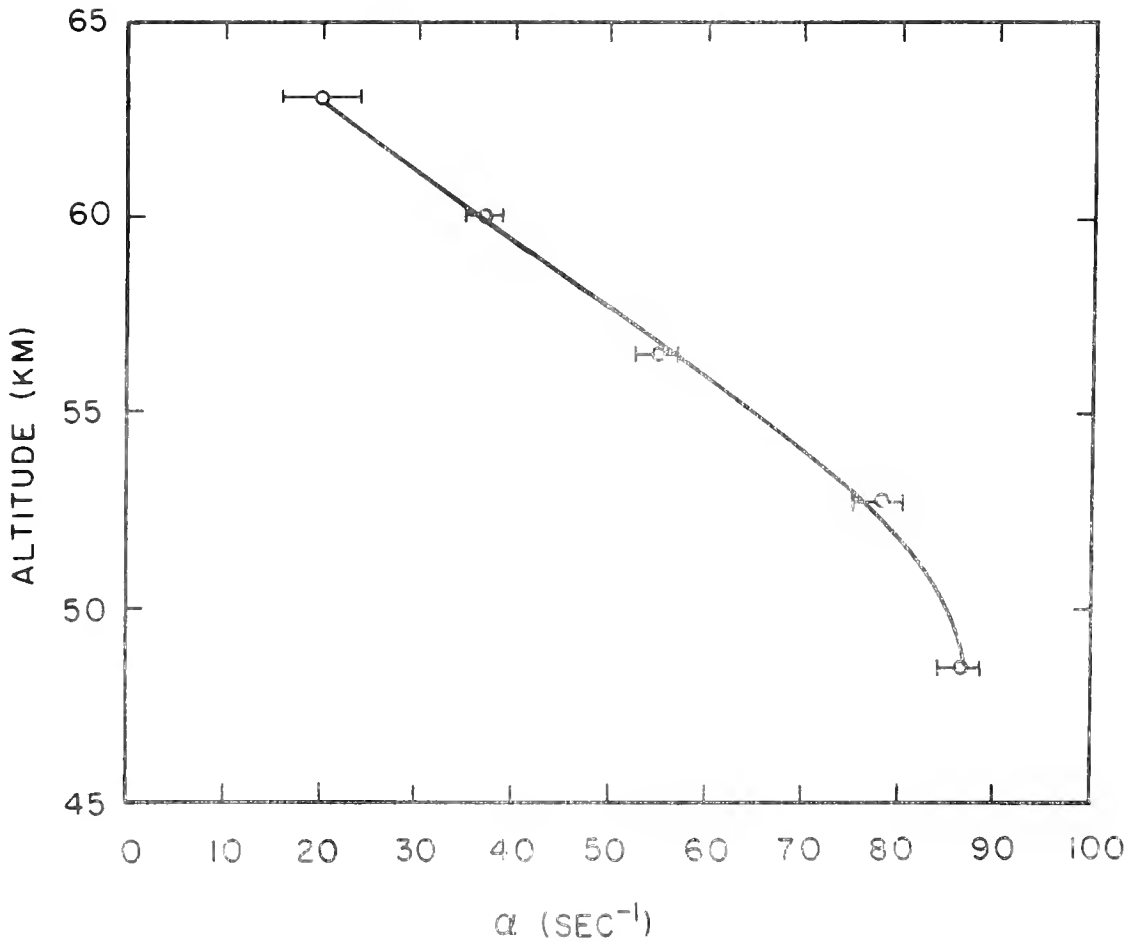

Figure 10. Attachment rate α from GIRE-I flight of 1 May 1962.

general agreement that the positive ion density is the order of $10^4 cm^{-3}$ at 60 km. Since there are probably less than 10^2 cm^{-3} electrons at this altitude in the daytime (under quiet sun conditions), a value of $\lambda \cong 10^2$ is necessary. This tends to support the fast electron removal rates indicated by the GIRE-I data.

As added proof of the foregoing explanation, two facts should be mentioned. First, there was some cross-modulation of the 225 Mc telemetry signal amplitude due to the gyrofrequency pulses during the part of the flight in question. As was indicated in Figure 5, the antennas for this telemetry transmitter were located near the gyrofrequency antenna feed points. It is unlikely that cross-modulation at 225 Mc would have occurred unless excess electrons were produced by each gyrofrequency pulse over a region several wavelengths (at 225 Mc) in size. The 234 Mc telemetry signal, which used a tail notch antenna, was not noticeably affected until after deployment of the gyrofrequency whip antennas.

A second observation is related to the GIRE-II data, which is yet to be discussed. However, an observation which pertains to this subject is that with the loop antenna used for the gyrofrequency pulses no cross-modulation was observed in the 60 km region. One earlier conjecture regarding the mechanism responsible for the apparent wave rotation in the GIRE-I data was that it was due to an electron spin population inversion in some paramagnetic constituent of the atmosphere, such as atomic oxygen. If this had been the case, the effect would have been enhanced with the strong RF magnetic fields, at approximately the Larmor frequency, radiated from the loop antenna in the GIRE-II payload. Its absence in the second experiment supports the conjecture that the effect was due to locally increased electron densities.

5.2 GIRE-II

The payload for the second experiment, GIRE-II, was designed primarily to study weak gyro-interaction effects. Of interest was the collisional energy loss rate for electrons with excess energy, a quantity commonly designated $G\nu$. The number G is the fraction of energy lost by an electron upon collision with a gas molecule, and ν is the collision frequency. These are related to electron temperature T by the well-known differential equation

$$\frac{dT}{dt} = - G\nu \, (T - T_o) \tag{5.63}$$

where T_o is the gas temperature.

To produce weak disturbances of electron energy a loop antenna was used for the gyrofrequency pulses. A block diagram of the GIRE-II payload is shown in Figure 11 and the antenna locations in Figure 12. The cross-modulation technique was used as with GIRE-I to detect the disturbances produced by the gyrofrequency pulses. While it was assumed that the disturbances would be weak, this conjecture was tested by the inclusion of measurements of excitation light and of gyrofrequency antenna voltage and in-phase current.

Cross-modulation data obtained from this flight had two forms. Below the reflection level of the 2.02 Mc sensing wave the cross-modulation was typical of that detected in a Luxembourg effect experiment. Above this level (97 km) all propagation of electromagnetic waves at 2.02 Mc was stopped by the cutoff nature of the magnetoplasma. Here the receiver input was due only to plasma noise; cross-modulation of this noise was observed.

A new type of RF probe designed to detect the frequency dependence of the real part of antenna impedance was included. Its purpose was to provide rapid measurements of electron density and collision frequency.

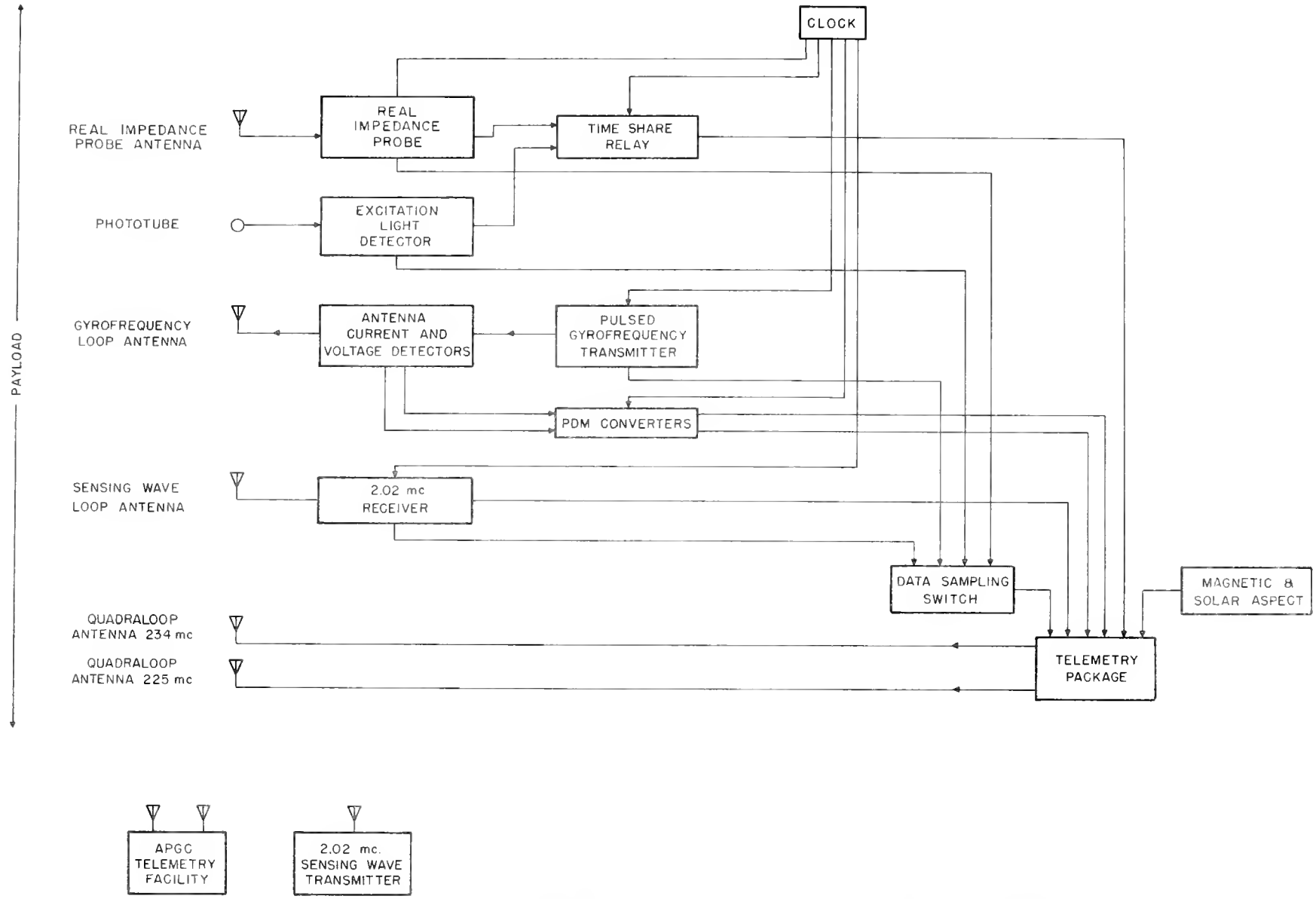

Figure 11. Block diagram of second gyro-interaction experiment showing both payload and ground support equipment.(GIRE-II)

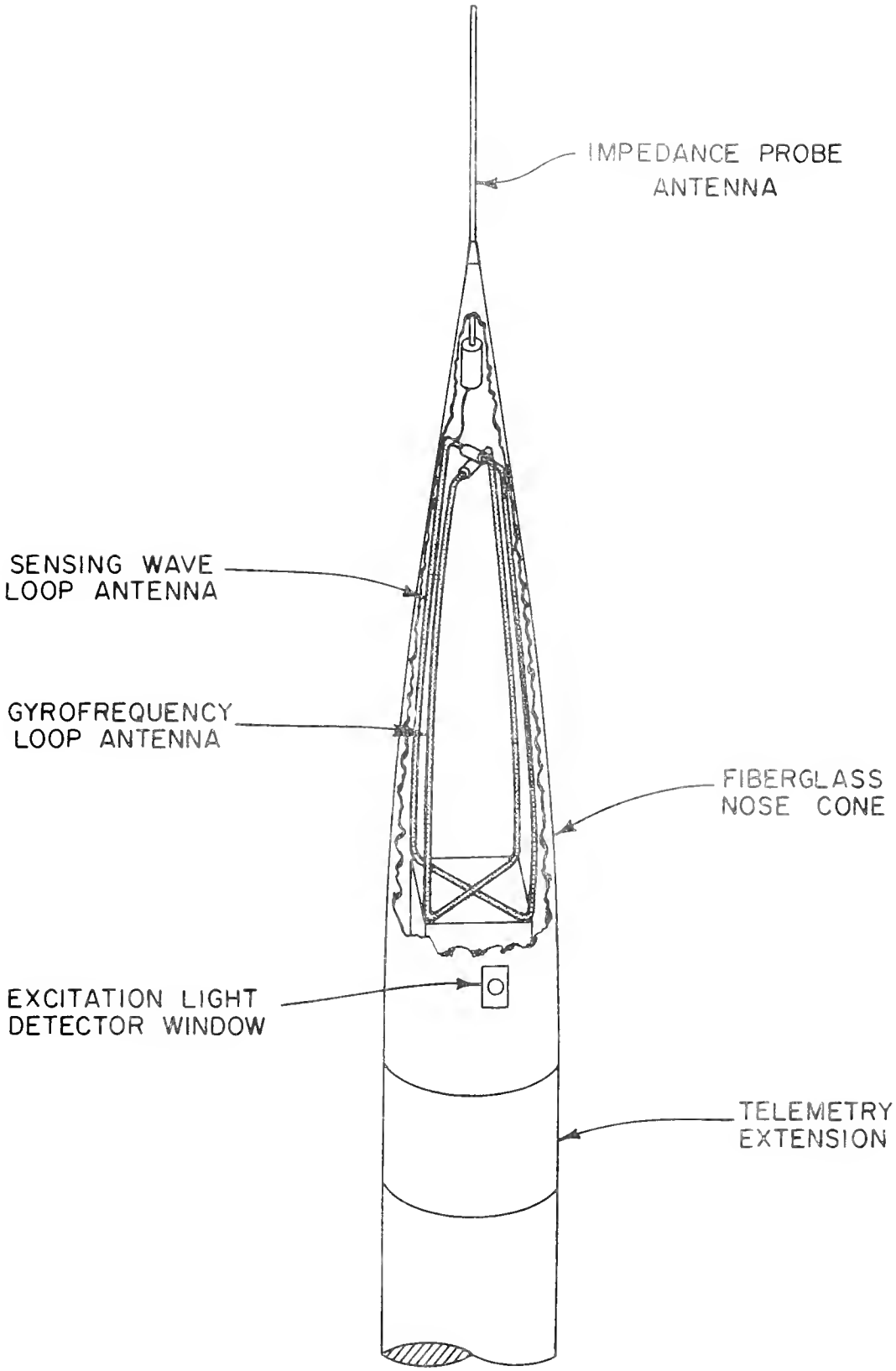

Figure 12. Locations of antennas for GIRE-II payload.

5.2.1 Flight Information

The relatively low maximum altitude attained by the GIRE-I payload (93.5 km) was ideal for these experiments; however, that flight used the last of the now obsolete Aerobee AJ 10-25 sustainers. As there was no suitable replacement, it was necessary to use an Aerobee 150 rocket for the GIRE-II flight. A sketch of the vehicle configuration is shown in Figure 13. The two inch severence ring contained a 110 pound lead ballast to bring the payload weight up to 300 pounds. This is the maximum allowable weight based on stress considerations. The 10 inch aspect extension contained solar and magnetic aspect sensors and a two-axis free gyroscope. This package was a prototype aspect system constructed by Spectral Physics Corp. for AFCRL; it was included by AFCRL to provide attitude information and to flight test the unit.

The GIRE-II payload was launched on 29 June 1963 at 1047 hours CST. The launch site was the same as for the first experiment. A plot of the trajectory obtained from radar tracking data is shown in Figure 14. The bearing at impact was 163.5° true; the maximum altitude was 157 km.[26]

5.2.2 Gyrofrequency Disturbance Pulses

The gyrofrequency transmitter was capable of delivering 100 watts peak power into a matched load. The loop antenna, with $Q = 50$, served as part of the final amplifier tank circuit. Since exact knowledge of the impedance of a loop antenna in a magnetoplasma was lacking, it was estimated that the loading of the antenna due to the ionosphere would still result in $Q > 10$ for the loop. The maximum power of 100 watts refers to a load which would make $Q = 10$. Alternate pulses were suppressed to give an available power of 10 watts into this load. The pulse repetition time was 100 milliseconds; the pulse width was 600 microseconds.

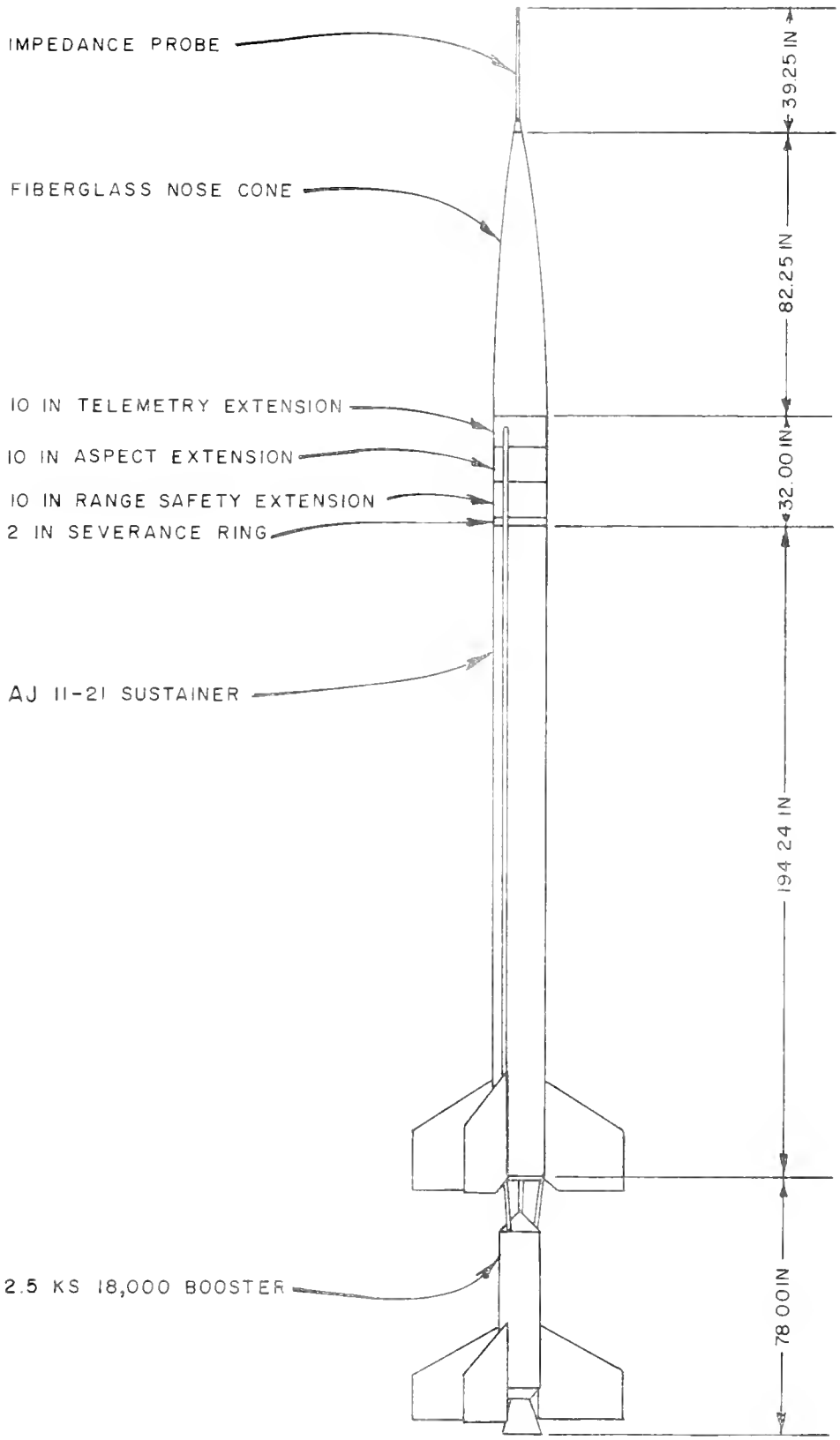

Figure 13. Vehicle configuration for GIRE-II.

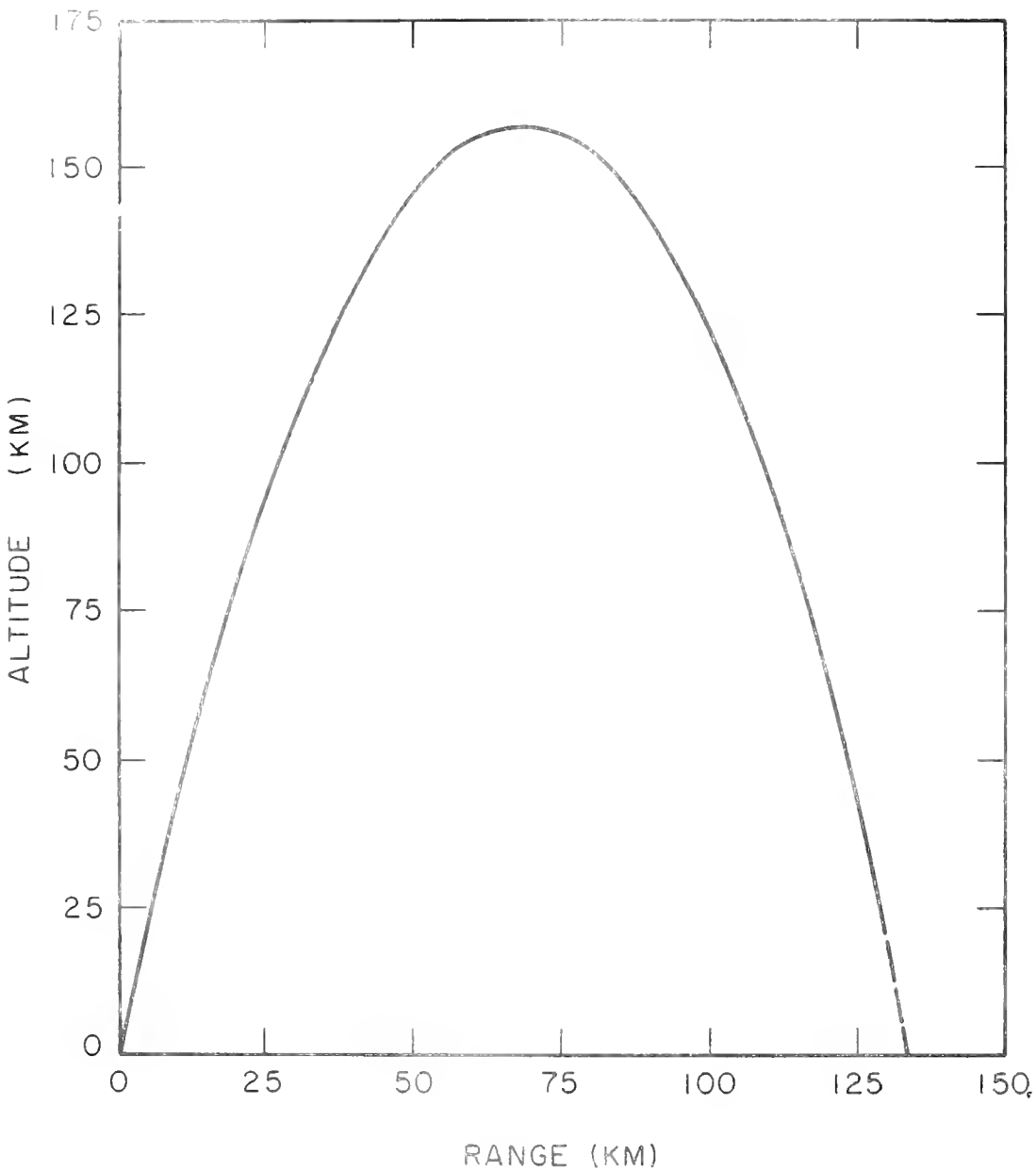

Figure 14. Trajectory of GIRE-II (1047 CST 29 June 1963). The bearing to the point of impact was 163.5° true.

With the loop antenna unloaded the antenna losses were responsible for dissipating 39 watts for the high-power output Estimating that the efficiency of the antenna in free space was $\sim 10^{-6}$, the radiated power would have been about 40 microwatts.

Provision was made to monitor the antenna voltage and in-phase current. In each 600 microsecond gyrofrequency pulse four samples of voltage and in-phase current were made. These were equispaced in time and had widths of 50 microseconds. Each sample was converted into a pulse of variable length with the use of pulse duration modulation (PDM) encoders. Thus for each gyrofrequency pulse the real impedance and power were measured four times.

These data show a negative result. No detectable change in the measured quantities occurred over the entire flight. For a measurement accuracy of roughly $\pm$ 1% the data indicates only that the radiating efficiency in the ionosphere never exceeded 10^{-2}. This leaves a range of uncertainty in efficiency of 10^{-6} to 10^{-2} or in radiated power of 40 microwatts to 0 4 watts

The excitation light detector consisted of a photomultiplier tube with S-11 response. It was situated at the end of an 8 inch long collimating pipe with 0.75 inch inside diameter. The data shows no excitation light This is submitted as evidence that each gyrofrequency pulse produced only a slight modification of electron temperature.

5.2.3 Cross-Modulation of Sensing Wave

The sensing wave transmitter, receiver, and antennas for GIRE-I and GIRE-II were almost identical. The receiver and loop antenna designs were modified slightly, resulting in a decreased output bandwidth of 7.5 kc (from 10 kc for GIRE-I). This was done to make the data more compatible with the telemetry system. The 7.5 kc bandwidth output was biased so that the telemetry ampli-

tude range of 0 to 5 volts corresponded to ± 25% fluctuation of the RF input voltage. Six equispaced segments of a data sampling switch (IRIG 30 x 5 standard format) were used to telemeter the full amplitude range of the receiver output at a rate of 30 samples per second. The AGC voltage was also telemetered at the 30 samples per second rate. In addition the portion of the AGC characteristic which changed least with input voltage was expanded by a dc amplifier and sampled at a rate of 15 times per second.

As was stated in Section 4, cross-modulation due to the modification of collision frequency in some disturbed region requires that the absorption index under normal conditions be sufficiently large and dependent on collision frequency. When the ratio of collision frequency ν to angular frequency ω is small, the absorption index χ for propagation of the sensing wave along the magnetic field is given by the Appelton-Hartree formula to be

$$\chi \cong \frac{N e^2}{2m\epsilon_o \omega^2} \left(\frac{\nu}{\omega \pm \omega_H} \right) \qquad (5.64)$$

where N is electron density, e and m are electronic charge and mass respectively, and ω_H is the angular gyrofrequency. Since χ is proportional to both N and ν it is evident that both are important. During the GIRE-II flight D region electron densities were so slight that the ordinary component of the sensing wave received negligible attenuation. A strong component was reflected by the sharp bottom of the E region resulting in a large standing wave. The motion of the rocket caused the receiver to detect this standing wave as a sinusoidal variation at the output. In many places the excursions were greater than the ± 25% amplitude range of the telemetry channel. Cross-modulation was observed only from 92 km to the reflection level at about 97 km during ascent. In

descent the period of the standing wave was very nearly one-half the gyrofrequency pulse repetition rate. Most gyrofrequency pulses occurred during either maxima or minima of the standing wave when one of the amplitude limits of the telemetry subcarrier oscillator was exceeded.

The data which was obtained during ascent is characteristic of that from a Luxembourg effect type of experiment. There is a sharp decrease in the sensing wave during the gyrofrequency pulse followed by an almost exponential return to the undisturbed condition. Figure 15 shows a portion of this data near 96.2 km during ascent. Since the disturbances were weak during this experiment, it is reasonable that the dimensions of each was fairly large. With the lack of a more complete knowledge of the extent of the gyro-interaction, it will be assumed that the gradient of electron temperature was sufficiently small everywhere to permit the use of the wave propagation (or WKB) approximations. With this conjecture the explanation of the data is that a gyrofrequency pulse caused an increase in electron temperature and hence in collision frequency. This resulted in increased absorption because of the linear dependence of χ, in Equation (5.64), on ν. At the end of the gyrofrequency pulse electron temperature began to return to equilibrium with the gas in a manner described by Equation (5.63). Thus these results may be interpreted in terms of the rate coefficient for loss of excess electron energy $G\nu$.

It is generally accepted that the collision frequency ν in air is proportional to electron temperature, or

$$\nu = \nu_o \left(\frac{T}{T_o}\right) \tag{5.65}$$

where the subscript o indicates equilibrium conditions. If G is assumed to be

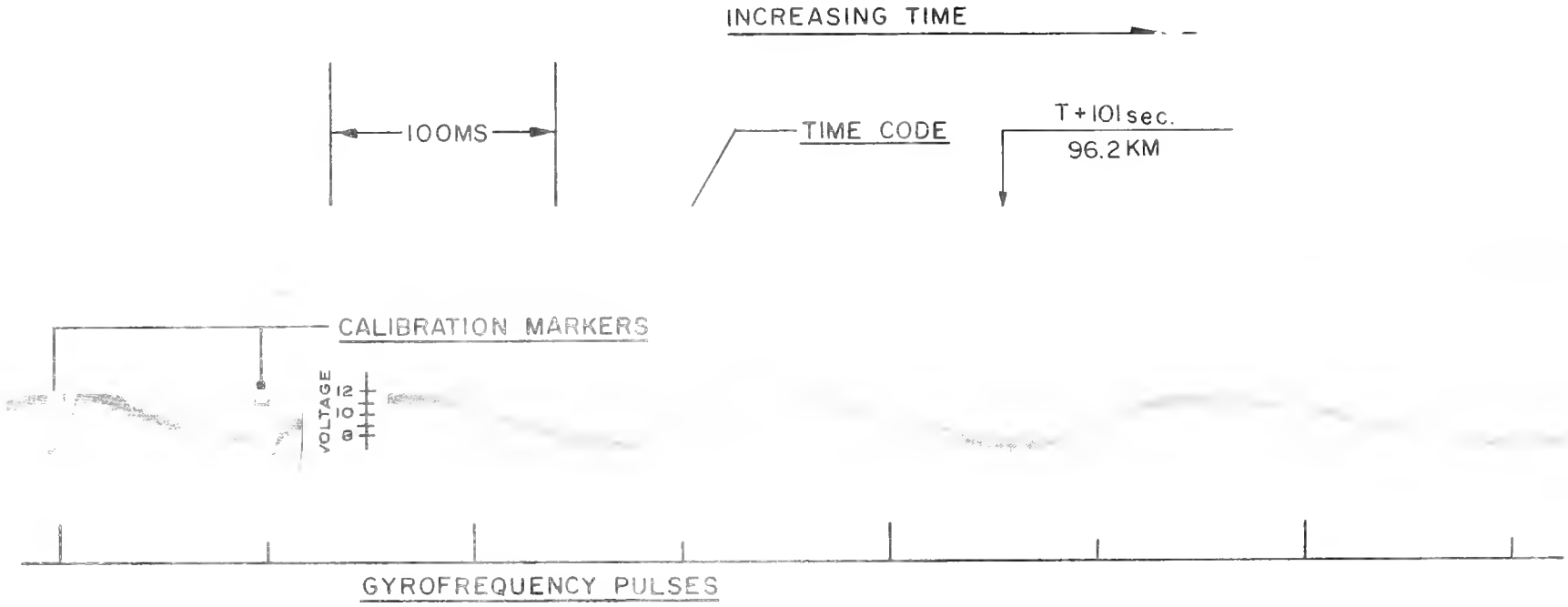

Figure 15. Sensing wave receiver output near 96.2 km during ascent.

a constant and ν in Equation (5 63) is replaced by Equation (5 65), the electron temperature behaves as

$$\frac{T(r,t)}{T_o} = \frac{1}{1 - (1 - \frac{T_o}{T_+(r)})e^{-G\nu_o(t-t_+)}} \qquad (5\ 66)$$

where $T_+(r)$ is the electron temperature at the end of the gyrofrequency pulse (i.e., at time t_+) at the position r. The spatial variation of T_+ is due to its dependence upon the gyrofrequency electric field intensity.

Absorption of the sensing wave is affected by electron temperature to the extent that the absorptive index, Equation (5.64), depends on collision frequency. Using Equation (5 65)

$$\chi(r,t) = \chi_o \frac{T(r,t)}{T_o} \qquad (5\ 67)$$

where χ_o is the equilibrium absorptive index and is presumed independent of r and t over the disturbed region.

The AGC time constant of the sensing wave receiver was greater than 100 milliseconds while the data shows decay times of only a few milliseconds. Thus AGC action may be neglected; and the receiver output can be expressed

$$V \simeq V_o \exp\left[-\frac{\omega}{c}\chi_o \int_p \left(\frac{T(r,t)}{T_o} - 1\right) dz\right] \qquad (5\ 68)$$

where V_o is the output voltage in the absence of the disturbance and p is the ray path of the sensing wave to the receiving antenna.

At $t = t_+$ the time derivative of Equation (5.68) is

$$\left(\frac{dV}{dt}\right)_{t_+} \simeq \frac{V_+}{V_o}\left(\frac{dV_o}{dt}\right)_{t_+} - V_+ \frac{\omega}{c}\chi_o \int_p \left[\frac{d}{dt}\ \frac{T(r,t)}{T_o}\right]_{t_+} dz \tag{5.69}$$

However, the rate at which V_o in the GIRE-II data changes is due primarily to the rocket motion through the standing wave composed of the incident and reflected components of the sensing signal. This varies slowly and hence

$$\frac{V_+}{V_o}\left(\frac{dV_o}{dt}\right)_{t_+} \simeq \frac{V_+}{V_-}\left(\frac{dV_o}{dt}\right)_{t_-} \tag{5.70}$$

where the subscript (-) refers to a condition just prior to the gyrofrequency pulse. The time derivative of Equation (5.66) at $t = t_+$ is

$$\left[\frac{d}{dt}\ \frac{T(r,t)}{T_o}\right]_{t_+} = -G\nu_o \frac{T_+(r)}{T_o}\left(\frac{T_+(r)}{T_o} - 1\right) \tag{5.71}$$

Combining Equations (5.69), (5.70), and (5.71) gives

$$G\nu_o = \frac{\left(\frac{dV}{dt}\right)_{t_+} - \frac{V_+}{V_-}\left(\frac{dV}{dt}\right)_{t_-}}{V_+ \frac{\omega}{c}\chi_o \int_p \frac{T_+(r)}{T_o}\left(\frac{T_+(r)}{T_o} - 1\right) dz} \tag{5.72}$$

Now, by utilizing Equation (5.68) with $t = t_+$, Equation (5.72) becomes

$$G\nu_o = \left[\frac{\left(\frac{dV}{dt}\right)_{t_+} - \frac{V_+}{V_-}\left(\frac{dV}{dt}\right)_{t_-}}{V_+ \ln \frac{V_-}{V_+}}\right] \cdot \frac{\int_p \left(\frac{T_+(r)}{T_o} - 1\right) dz}{\int_p \frac{T_+(r)}{T_o}\left(\frac{T_+(r)}{T_o} - 1\right) dz} \tag{5.73}$$

As was mentioned previously, $T_+(r)$ is not known. However, note that since $T_+(r) > T_o$ everywhere,

$$\int_p \left(\frac{T_+(r)}{T_o} - 1 \right) dz \leq \int_p \frac{T_+(r)}{T_o} \left(\frac{T_+(r)}{T_o} - 1 \right) dz \qquad (5\text{-}74)$$

Therefore, $G\nu_o$ has an upper bound i.e.,

$$G\nu_o \leq \frac{\left(\frac{dV}{d\tau}\right)_+ - \frac{1}{V_-}\left(\frac{dV}{d\tau}\right)_+}{V_- \ln \frac{1}{V_-}} \qquad (5\text{-}75)$$

It can be shown that Equation (5-75) is the exact expression obtained when ν is assumed to be independent of electron temperature for which the solution to Equation (5-63) is an exponential decay of temperature.

In the previously cited work of Fejer[4] ν was assumed to be independent of temperature, and values of $G\nu_o$ and of G were found, from which a curve of ν versus altitude was deduced. Reversing the process and using Fejer's value of $G = 10^{-2}$ gives the $G\nu_o$ curve shown as a solid line in Figure 16. This data has a stated accuracy of $\pm$ 40%. The GIPE-II data are also plotted on this graph as circles. These values were obtained by using expression (5-75) as an approximation. There is close agreement between the present data and the extrapolation of the curve from Fejer, both of which are based on the same assumption; that excess electron temperature decays exponentially.

The foregoing treatment was based on the assumption that with each gryofrequency pulse the electron temperature was increased slightly in some region surrounding the rocket. An intense heating of the electrons near the rocket would probably have been accompanied by excitation light and a change in the gyrofrequency antenna impedance, that neither of these was detected supports

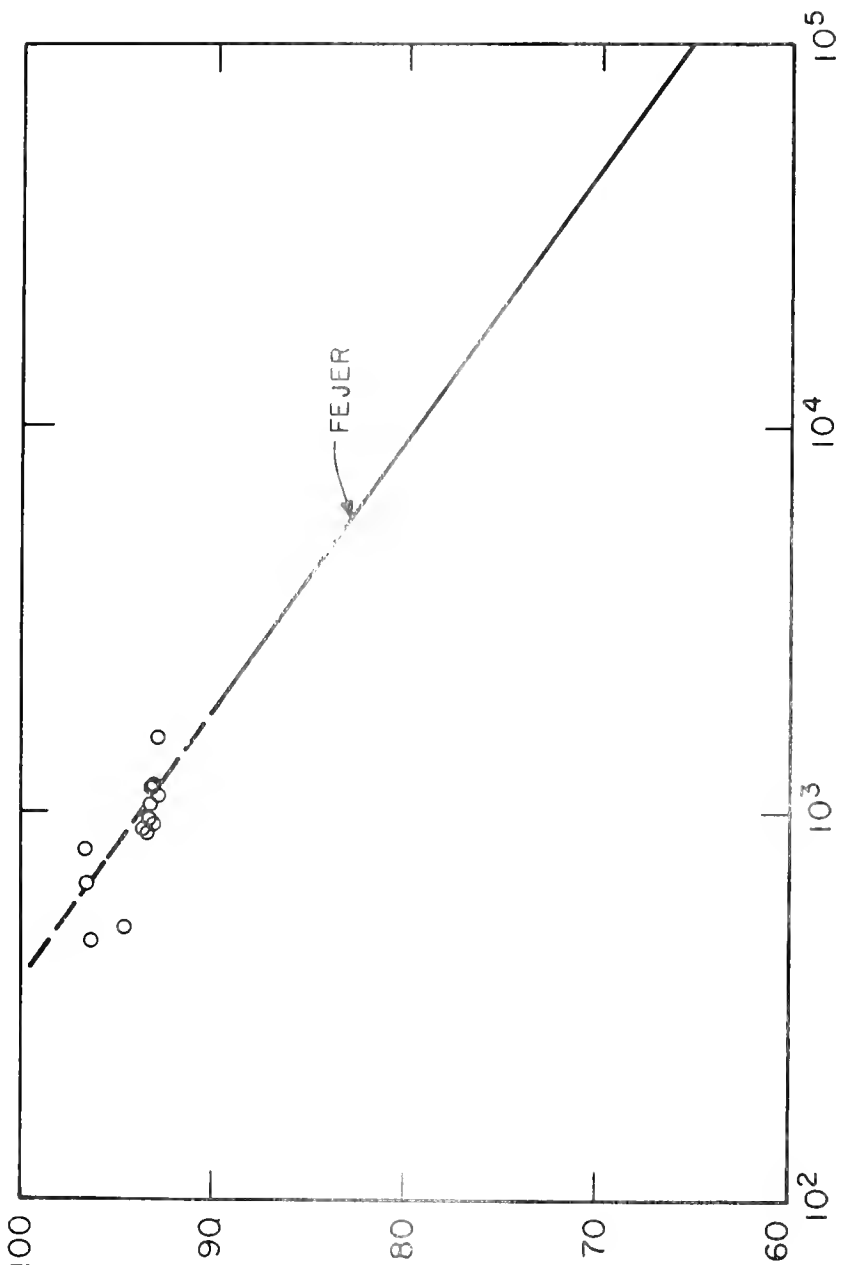

Figure 16. $G\nu_o$ from sensing wave cross modulation from GIRE-II (indicated by circles). Solid line is from Fejer[4].

the assumption that the elctron temperature near the rocket was not greatly changed. As can be seen in Figure 15 the cross-modulation was typically a 25% decrease in the receiver output. At 96 km the approximate plasma parameters for the sensing wave frequency are: electron density $N \simeq 7 \times 10^4$ cm^{-3}; and $\nu \simeq 10^5$ sec^{-1}. With the use of these values the observed cross modulation would be given by Equation (5.68) if initially the disturbances were the equivalent of an average increase of electron temperature by a factor of 2 within 1000 meters of the rocket. This is not an unreasonable requirement

5.2.4 Plasma Noise Measurements

As the GIRE-II payload was carried through the ionosphere, it crossed the various reflection levels for the different sensing wave components The highest of these would have been that for which

$$X = 1 - Y \qquad (5.76)$$

For X greater than this value the index of refraction for all waves and all directions of travel, as given by the lossless Appelton-Hartree formula, is imaginary. The inclusion of losses does not change the situation significantly If the plasma, or acoustic, waves are considered,[27] the electron plasma wave is also cut off Neglecting Landau damping the ion plasma wave could propagate; but since the wave velocity and mean ion thermal velocity are nearly equal for this wave, Landau damping should cause severe attenuation Therefore, in this region the 2 02 Mc receiver input could have been due only to locally produced plasma noise

Several interesting observations can be made from the plasma noise measured during the GIRE-II flight The receiving loop antenna detected the H field, and thus the AGC voltage gives an equivalent free space E field

(i.e., 377 Ω). Plots of the receiver AGC records during ascent and descent through the reflection region are shown in Figure 17. In ascent the trajectory of the rocket carried it through a region where part of the sensing wave penetrated the X = 1 altitude. Complete reflection occurred at the X = 1 + Y height. (Because of the AGC time constant the true rate of change in field strength with altitude is not given by the AGC voltage.) Above this reflection point the receiver input dropped to the plasma noise level.

During descent the amplitude of the noise input dropped abruptly at 97 km, the altitude corresponding to X = 1 + Y. While the medium was no longer cutoff, the input was not due to the sensing wave but to receiver, antenna, and atmospheric noise. The coherent sensing signal was only detected below 92.5 km. That the sensing wave did not penetrate above this altitude is understandable from the nature of the reflection of a wave incident upon the ionosphere at a shallow angle. As can be seen from Figure 14 the angle of incidence of the sensing wave was less than 45° in this area. In such a case the reflection is a gradual process due to the gradient of electron density and hence of the refractive index. Thus, complete reflection was achieved below the X = 1 level.

One interesting aspect of this record is that the cutoff plasma noise spectral density was significantly greater than receiver, antenna, or atmospheric noise. If the plasma noise source were due to equilibrium radiation within the ionosphere, it could be described in terms of the antenna temperature, i.e., as Johnson noise. It is known that the free space efficiency of the receiving loop antenna was less than 10^{-6}. The similar gyrofrequency transmitter loop had an efficiency in the ionosphere less than 10^{-2}. If we assume as the most favorable conditions for the production of noise that the receiving antenna efficiency reached 10^{-2} above 97 km and that antenna noise at 300° K

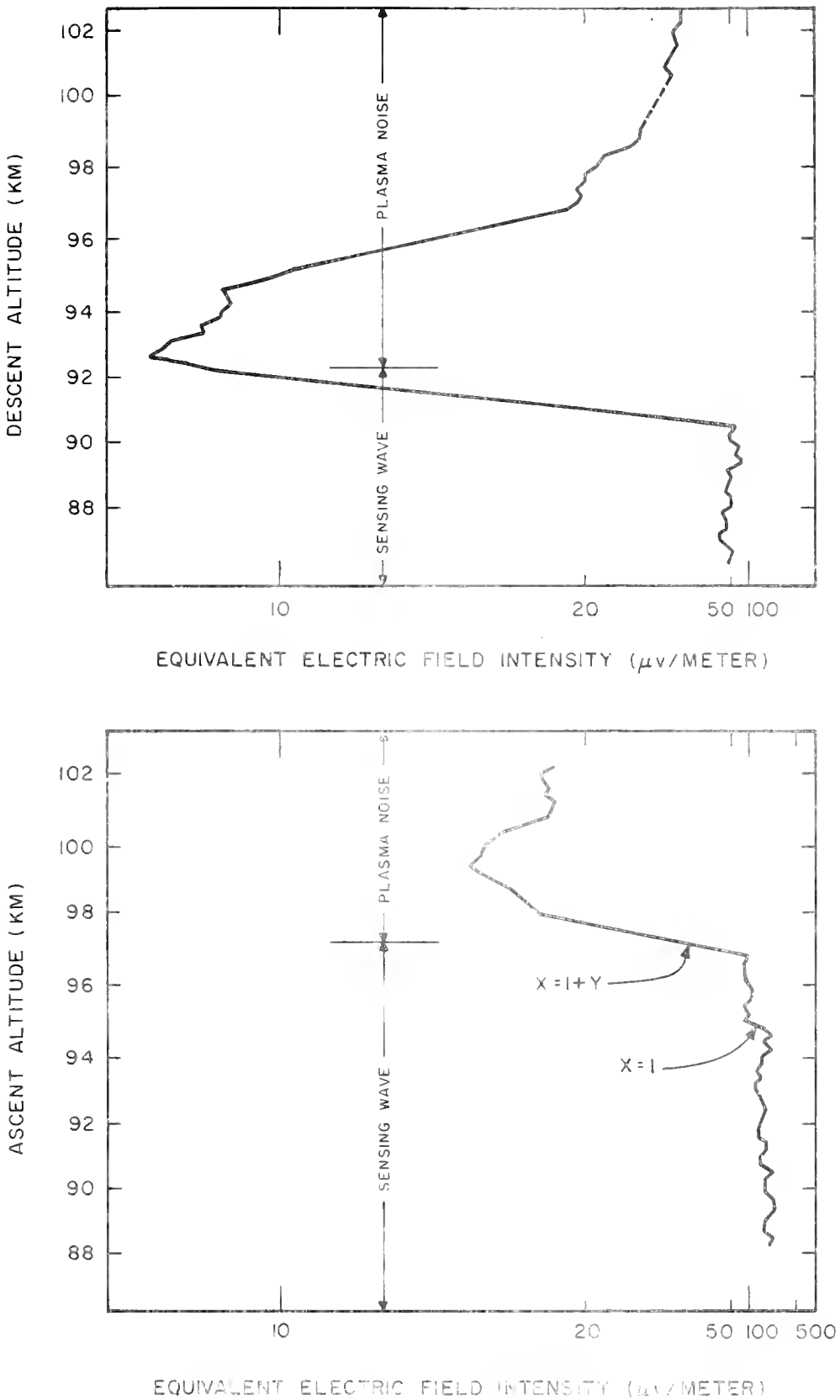

Figure 17. 2.02 Mc receiver AGC record through reflection region.

produced the 10 microvolt/meter noise near 94 km during descent, the plasma temperature above 97 km necessary to produce 30 microvolts/meter would have been at least 300,000° K. This calculation is very unrealistic and indicates that the process must involve some nonequilibrium conditions. The noise was of fairly constant amplitude over the entire trajectory above 97 km which would rule out the effects of ionospheric inhomogeneities, except perhaps that produced by the supersonic motion of the rocket.

A second observation regarding this noise is that there was a significant cross-modulation of the noise spectral density with each gyrofrequency pulse. Figure 18 shows a sample of the receiver output data near 106.4 km in ascent. It is interesting to note that the noise level decreased with each pulse and recovered several milliseconds later.

While the mechanism responsible for the noise is not understood, the dependence of the receiver input on electron temperature can be examined. It is postulated that the receiver rms input V is given by

$$V = C T^{-\gamma} \tag{5.77}$$

where C and γ are constants. The time derivative of V at the end of a gyrofrequency pulse (i.e., $t = t_+$) is then

$$\left(\frac{dV}{dt}\right)_{t_+} = -\frac{\gamma V_+}{T_+}\left(\frac{dT}{dt}\right)_{t_+} \tag{5.78}$$

Combining Equations (5.71) and (5.78) gives

$$G\nu_o = \frac{\left(\frac{dV}{dt}\right)_{t_+}}{\gamma V_+\left(\frac{T_+}{T_o} - 1\right)} \tag{5.79}$$

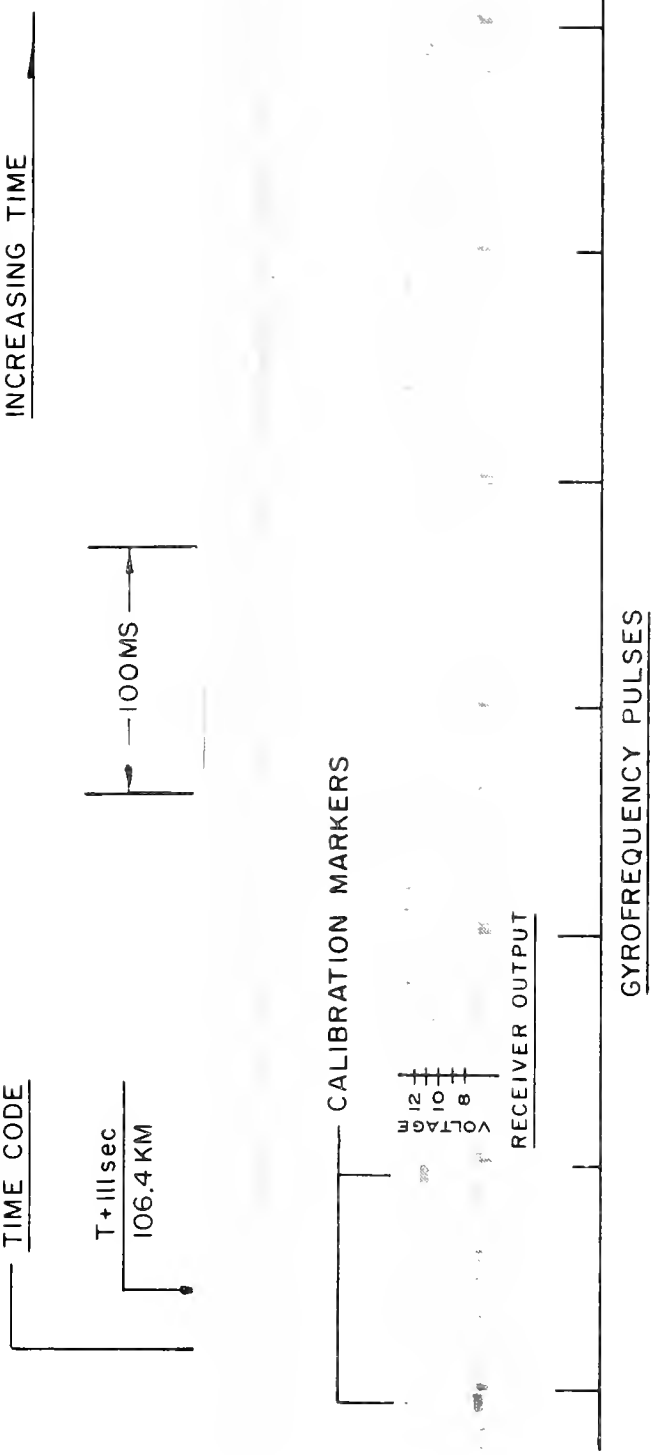

Figure 18. Cross-modulation of plasma noise near 106.4 km during ascent.

With the use of Equation (5.77) this becomes

$$G\nu_o = \frac{\left(\frac{dV}{dt}\right)_{t_+}}{\gamma V_+ \left[\left(\frac{V_-}{V_+}\right)^{1/\gamma} - 1\right]} \tag{5.80}$$

A number of the cross-modulation wave shapes have been interpreted via Equation (5.80) for various values of γ. Best agreement with a straight line extrapolation of the $G\nu_o$ measurement of Fejer[4] was found for $\gamma = 1/4$. These data and the curve from Fejer are shown in Figure 19.

The real impedance probe was periodically gated on and off throughout the flight. With a maximum antenna RF voltage of 0.5 volt and a current of 10 microampers there was sufficient energy radiated to produce cross-modulation of the plasma noise for longer durations. In each case the effect of the RF fields of the probe was to decrease the plasma noise input to the 2.02 Mc receiver. This supports the observation made from the gyrofrequency cross-modulation data that the noise spectral density decreased with increasing electron temperature.

5.2.5 Real Impedance Probe

The RF probe included in the GIRE-II payload was designed to measure the real part of the impedance of a short antenna over a range of frequencies. The impetus for the inclusion of such a device was the work of Balmain[28] on the impedance of a small antenna in a magnetoplasma. For a monopole of length L and radius ρ Balmain obtained the impedance formula

$$\mathcal{Z} = \frac{\ln \frac{L}{\rho} - 1 - \ln B_\theta}{j\omega\, 2\pi\, \epsilon_o\, L\sqrt{K_\theta K'}} \tag{5.81}$$

where $$K_\theta = K_o \sin^2\theta + K' \cos^2\theta \tag{5.82}$$

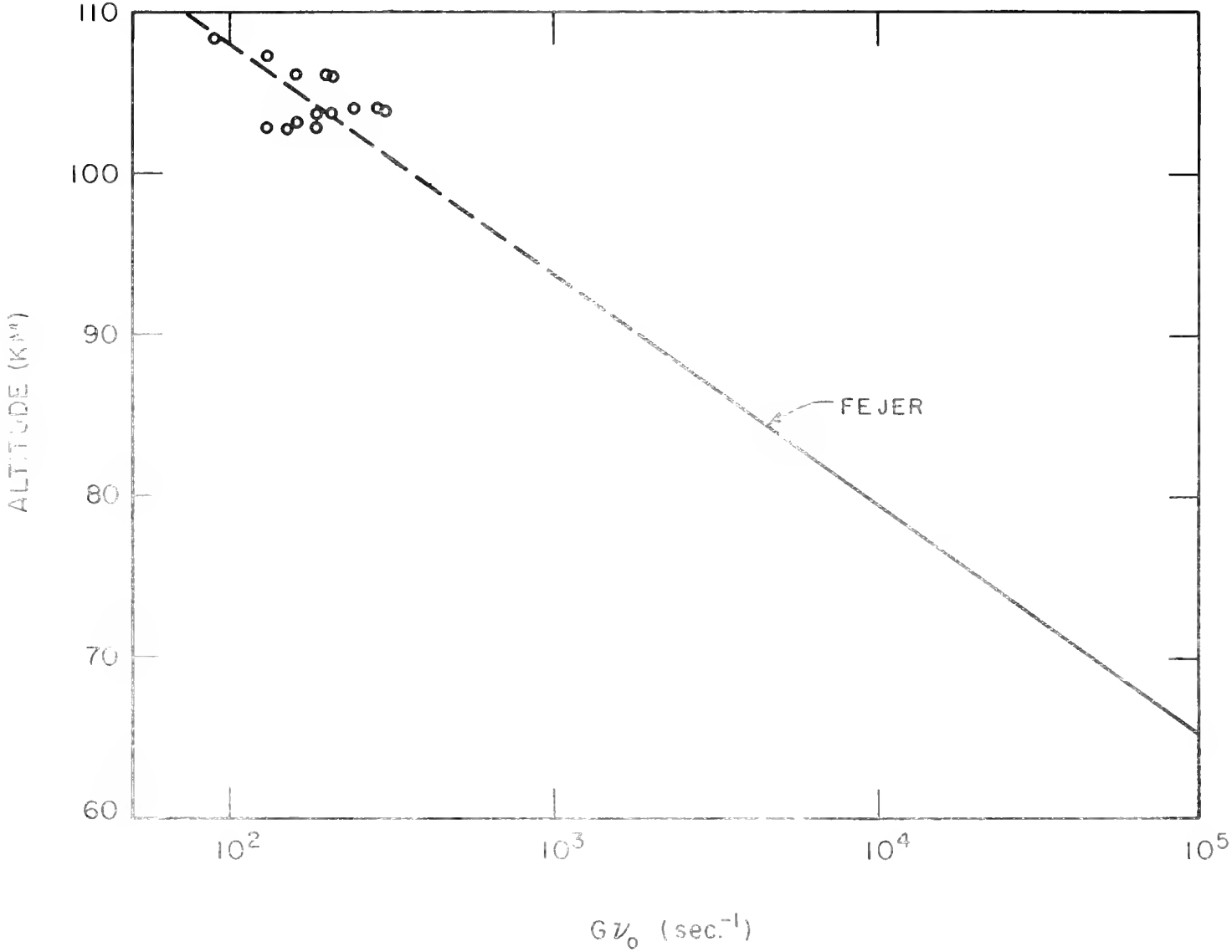

Figure 19. ν_o from noise cross modulation for $\gamma = \frac{1}{4}$ (indicated by circles). Solid line is from Fejer[4].

$$B_\theta = \frac{1}{2}\left\{\sqrt{\frac{K_o}{K_\theta}} + \sqrt{\frac{K' K_o}{K_\theta^2}}\right\} \tag{5.83}$$

The angle θ is that between the axis of the antenna and the magnetic field B_o. The coefficients K' and K_o are the diagonal terms of the permittivity tensor:

$$K' = 1 - \frac{XU}{U^2 - Y^2} \tag{5.84}$$

$$K_o = 1 - \frac{X}{U} \tag{5.85}$$

Expression (5.81) is an approximation based on the condition

$$\left(\frac{\rho}{L}\right)^2 << \left|\frac{K'}{K_o}\right| \tag{5.86}$$

For a collisionless plasma the ratio K'/K_o can be expressed

$$\frac{K'}{K_o} = \frac{f^2 (f^2 - f_o^2)}{(f^2 - f_N^2)(f^2 - f_H^2)} \tag{5.87}$$

where

$$f_o^2 = f_N^2 + f_H^2 \tag{5.88}$$

It is evident that for $f \cong f_o$ condition (5.86) is violated for the lossless case.

In the lower ionosphere the effect of collisions is not negligible. For the collision frequency data of Schlapp[29] and an assumed electron density of

approximately 1.2×10^5 cm^{-3}, condition (5.86) is valid for $\rho/L = 10^{-2}$ at altitudes below 120 km. However, it should be expected than an ion sheath would form about the probe, causing an increased effective radius. The effect of such a sheath in condition (5.86) is not accurately known.

For the special case $\theta = 0$, formula (5.81) has the form

$$\mathcal{Z}(\theta=0) = \frac{\ln \frac{L}{\rho} - 1 + \ln\sqrt{\frac{K'}{K_o}}}{j\omega\, 2\pi\, \epsilon_o\, L\, K'} \tag{5.89}$$

When condition (5.86) is satisfied, the frequency dependence of Equation (5.89) is most affected by a maximum of the real part of the inverse of K' at the angular frequency

$$\omega_o^2 \cong \omega_N^2 + \omega_H^2 - \nu^2 \tag{5.90}$$

In the absence of collisions this would reduce to Equation (5.88). In Figures 20a, b, c, and d the real and imaginary parts of $\mathcal{Z}(\theta=0)$ scaled by ω/ω_H have been plotted as functions of ω_o for various sets of parameters. These calculations were made for $\omega_H = 1.4$ Mc, $L = 1$ meter, and $\rho = 0.01$ meter. In each case the resonance width is approximately 2ν. From these curves it appears that if θ could be controlled by sweeping the applied frequency, it should be possible to determine both ω_o and ν from the resonance of the real part of antenna impedance.

A factor which limits the ability of a probe to measure ν is the effect of the fields of the probe on electron temperature and hence upon ν. It is well known that an electric field E will have negligible effect on electron

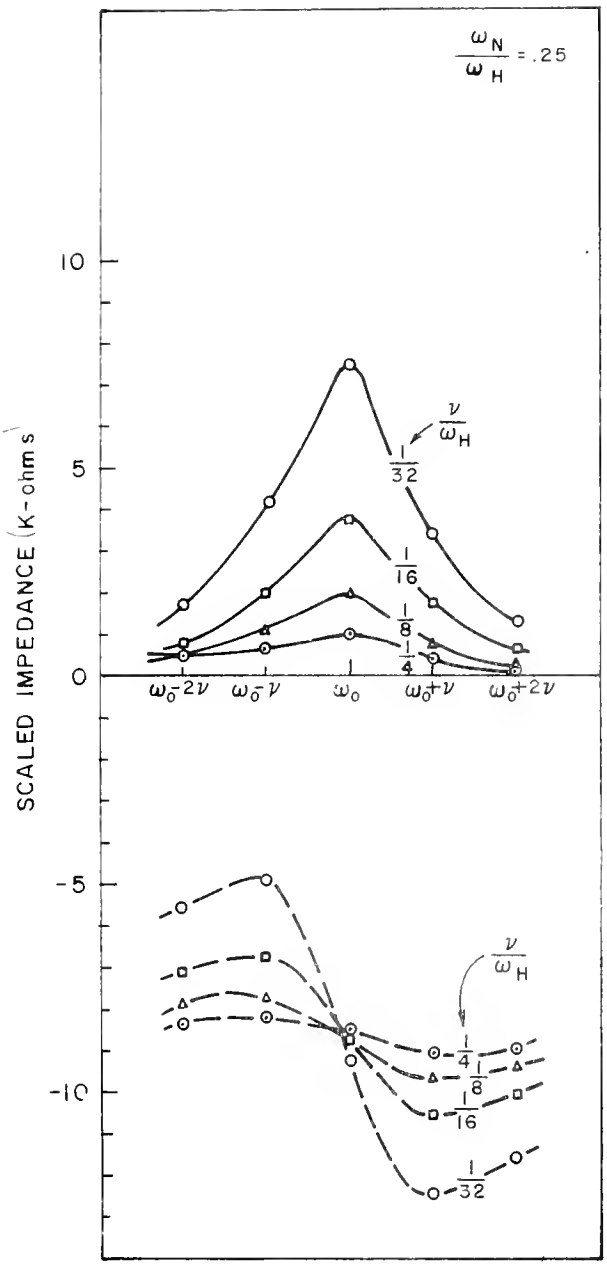

Figure 20a. Scaled real and imaginary parts of antenna impedance for $\frac{\omega_N}{\omega_H} = .25$

$\frac{\omega}{\omega_H}$ Re $\mathcal{Z}$: ————

$\frac{\omega}{\omega_H}$ Im $\mathcal{Z}$: - - - - -

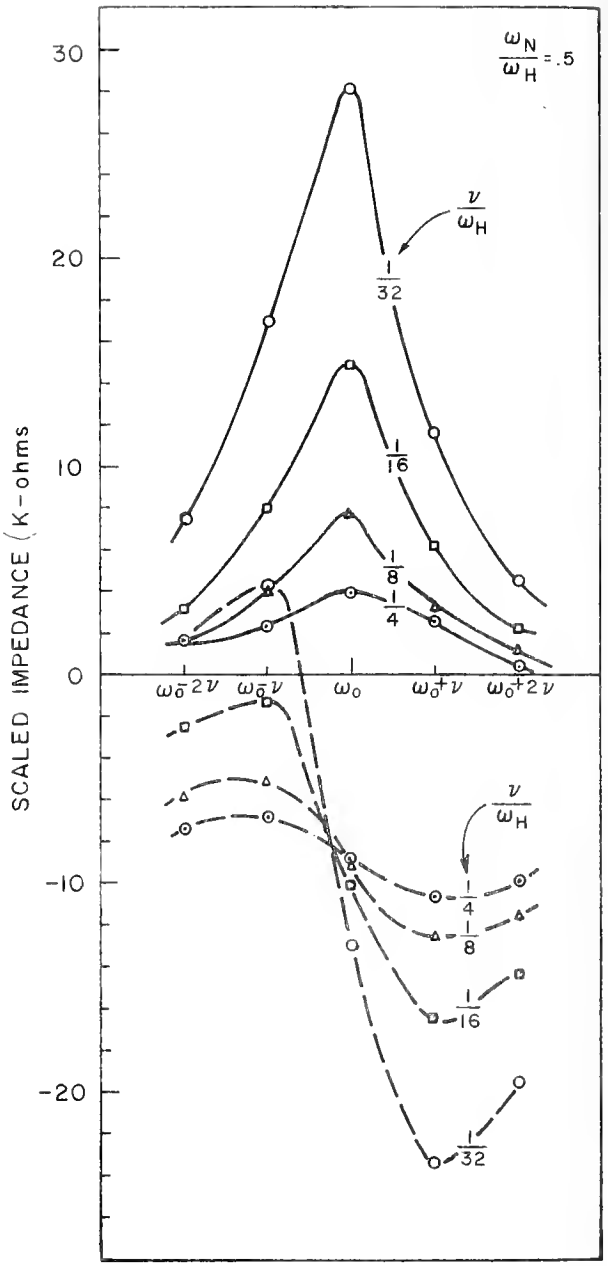

Figure 20b. Scaled real and imaginary parts of antenna impedance for $\frac{\omega_N}{\omega_H} = .5$

$\frac{\omega}{\omega_H}$ Re $\mathcal{Z}$: ————

$\frac{\omega}{\omega_H}$ Im $\mathcal{Z}$: - - - - -

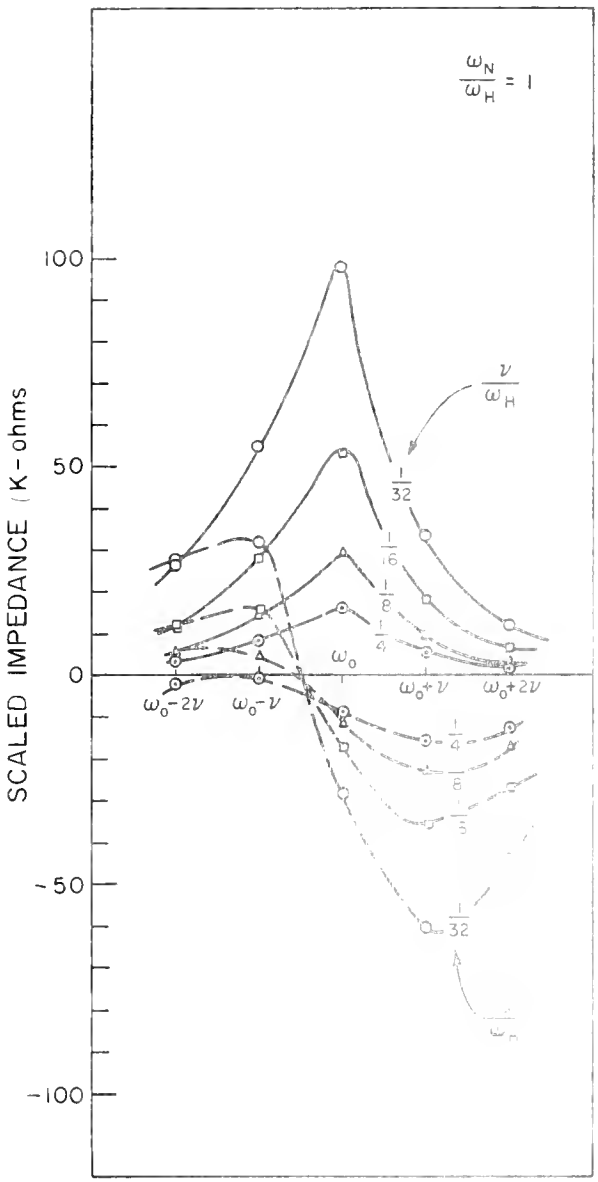

Figure 20c. Scaled real and imaginary parts of antenna impedance for $\frac{\omega_N}{\omega_H} = 1$

$\frac{\omega}{\omega_H}$ Re $\mathcal{Z}$: ————

$\frac{\omega}{\omega_H}$ Im $\mathcal{Z}$: - - - - -

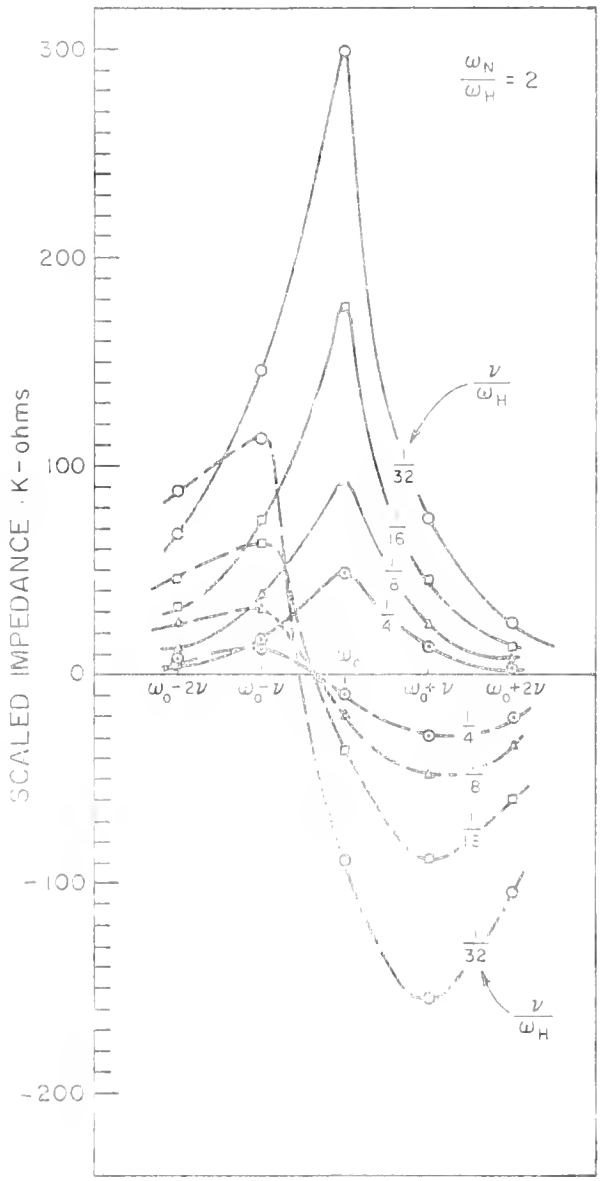

Figure 20d. Scaled real and imaginary parts of antenna impedance for $\frac{\omega_N}{\omega_H} = 2$

$\frac{\omega}{\omega_H}$ Re $\mathcal{Z}$ ————

$\frac{\omega}{\omega_H}$ Im $\mathcal{Z}$ - - - - -

temperature if

$$E << \sqrt{\frac{3\,k\,T\,m\,G}{2\,e^2}\left[(\omega - \omega_H)^2 + \nu^2\right]} \qquad (5.91)$$

where k represents Boltzmann's constant.[30] To instrument a device capable of measuring the range of impedances indicated in Figures 20a, b, c, and d, it was convenient to apply a constant RF current to the probe and to measure the in-phase component of voltage at the feed point. This necessitated a wide range of antenna voltages, the minimum being determined by noise considerations. As a consequence it was estimated that the usefulness of the device in measuring ν would be limited by condition (5.91) to altitudes below 90 km.

Because of the relatively low electron densities encountered during the GIRE-II flight, the only measurement of ν was near 88.5 km. The value obtained is $\nu = 3.6 \times 10^5$ sec^{-1}, with an electron density of 4×10^3 cm^{-3}. The resonance width of the probe data broadened with increasing altitude, indicating the presence of a loss mechanism in addition to collisions. Because of this the value of ν cited above should be regarded as an upper bound.

The broadening of the resonance may be ascribed to one or more of various mechanisms such as the excitation of acoustic plasma waves, or the ion sheath and the related removal of electrons by the antenna as in the Takayama probe.[31] While the exact mechanism is not known, the presence of the broadening makes it possible to observe discontinuities caused by abrupt changes in the argument of B_θ in Equation (5.81). In the following discussion it will be convenient to consider the lossless case for which K', K_o, and K_θ are simple fractions

$$K' = \frac{f^2 - f_o^2}{f^2 - f_H^2} \qquad (5.92)$$

$$K_o = \frac{f^2 - f_N^2}{f^2} \tag{5.93}$$

$$K_\theta = \frac{(f^2 - f_1^2)(f^2 - f_2^2)}{f^2(f^2 - f_H^2)} \tag{5.94}$$

where

$$f_{1,2}^2 = \frac{1}{2}\left\{f_o^2 \mp \sqrt{f_o^4 - 4f_N^2 f_H^2 \sin^2\theta}\right\} \tag{5.95}$$

and f_o^2 satisfies Equation (5.88). The general shapes of the magnitudes of the frequency dependent parts of $\mathcal{Z}$, Equation (5.81), are plotted in Figure 21. While the impedance formula is questionable near f_o, there is a very definite jump in the argument of B_θ at the plasma frequency f_N. Since

$$\ln B_\theta = \ln \left| B_\theta \right| + j\,(\arg B_\theta) \tag{5.96}$$

a change in $(\arg B_\theta)$ should contribute a corresponding change in the real part of $\mathcal{Z}$. As the frequency is swept through f_N, there should be a jump in the real part of $\mathcal{Z}$ regardless of θ.

Had the resonance data depended only on collisional losses, f_N would have been out of the resonance width over most of the flight, and the jump at f_N would have been indistinguishable from noise. However, the broadening of the resonance permitted this discontinuity to be observed as can be seen in a sample of the probe data shown in Figure 22. In the decreasing frequency part of the sweep there is an upward jump near the peak of the resonance and a downward jump corresponding to f_N on the slope. The discontinuity near the peak does not correspond exactly to f_2. The error may be due in part to the

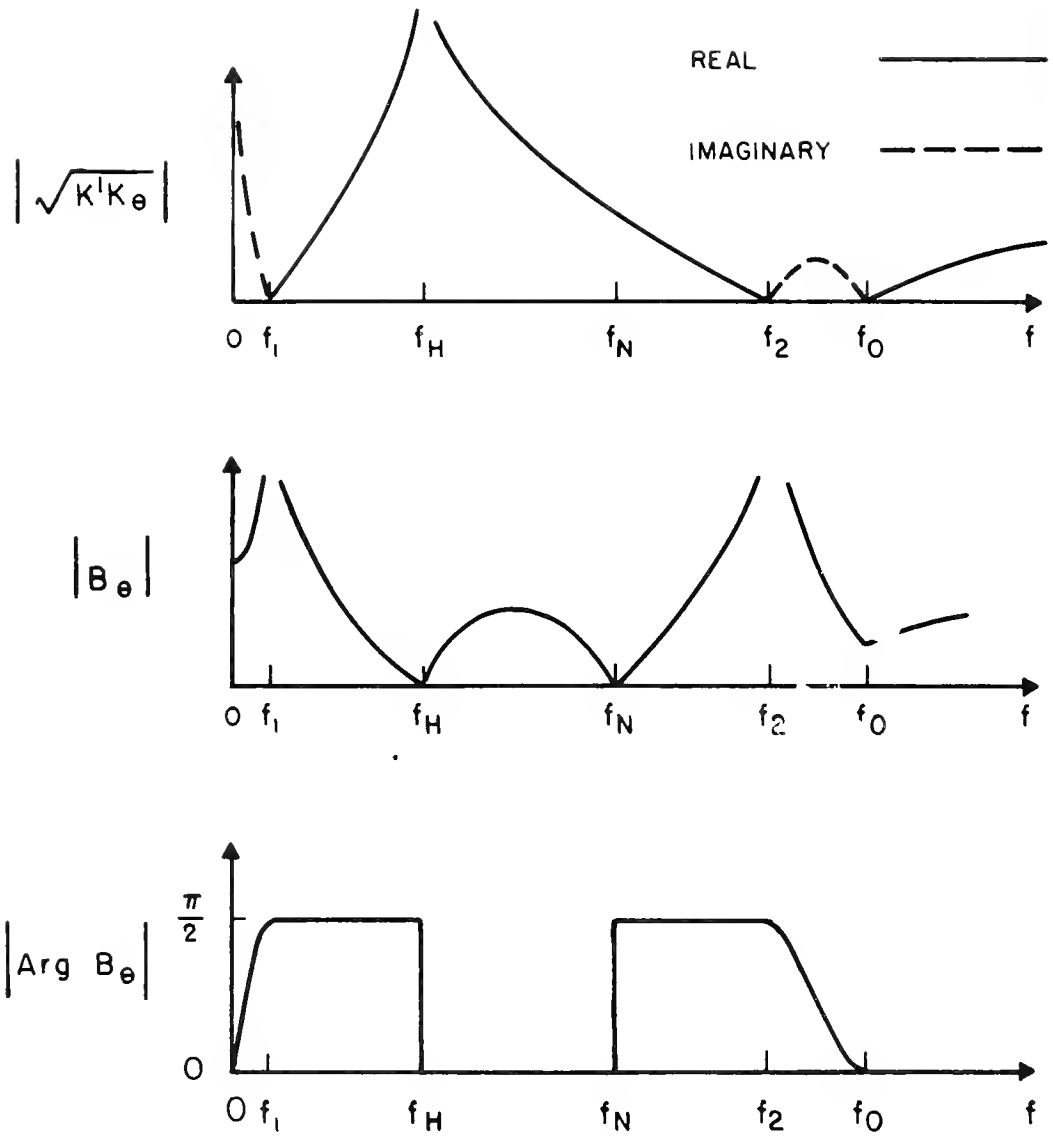

Figure 21. Approximate graphs of $\left|\sqrt{K'K_\theta}\right|$, $\left|B_\theta\right|$ and $\left|\arg B_\theta\right|$ for a lossless plasma.

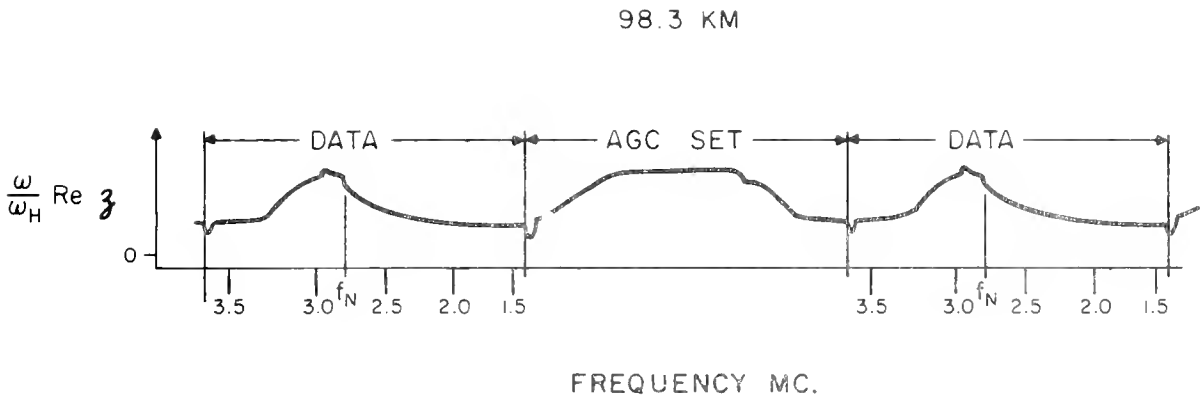

Figure 22. Real impedance probe data near 98.3 km during ascent (GIRE-II)

effect of the ion sheath on the effective radius of the probe. The increasing frequency part of the cycle was used for setting an AGC circuit to assure that the following resonance peack amplitude would be 4 volts for telemetry purposes. The duration of each sweep was 16 milliseconds.

Electron densities determined from the probe data are shown in Figure 23. All densities above 94 km are from plasma frequency discontinuities in the data. Below 94 km these discontinuities did not occur, presumably because $f_N < f_H$. Here the data represents plasma frequencies deduced by assuming that the resonance peaks occurred at f_o. Near 88 km the plotted data are averages over 10 consecutive measurements; near 91 km these are averaged over 5 points. Above 94 km all points (22 measurements per set) are plotted. The lack of continuity in the plotted densities is due to the 25% duty cycle of the probe. It was disabled part of the time to eliminate interference in the cross modulation measurements. There were several instances in which the probe provided no data during an entire period of operation. These are attributable to temporary confusion of the logic circuitry which controlled the sweep.

To assess the accuracy of the probe in measuring electron density the points corresponding to $X = 1$ and $X = 1 + Y$ from the sensing wave reflection level data have been plotted in Figure 23. These are in good agreement with the probe data.

One mission of the probe was to detect changes produced by the gyrofrequency pulses. This was the reason for the fast sweep time. As was the case for the measurements of gyrofrequency antenna impedance and excitation light, the probe data also indicates no detectable modification of either electron density or temperature near the rocket. This supports the assumption of very weak gyro-interaction effects.

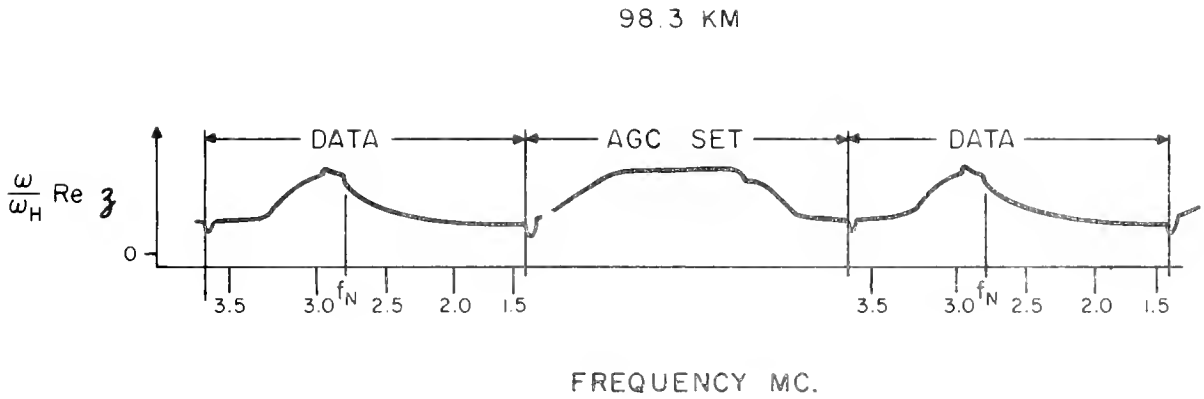

Figure 22. Real impedance probe data near 98.3 km during ascent (GIRE-II)

effect of the ion sheath on the effective radius of the probe. The increasing frequency part of the cycle was used for setting an AGC circuit to assure that the following resonance peack amplitude would be 4 volts for telemetry purposes. The duration of each sweep was 16 milliseconds.

Electron densities determined from the probe data are shown in Figure 23. All densities above 94 km are from plasma frequency discontinuities in the data. Below 94 km these discontinuities did not occur, presumably because $f_N < f_H$. Here the data represents plasma frequencies deduced by assuming that the resonance peaks occurred at f_o. Near 88 km the plotted data are averages over 10 consecutive measurements; near 91 km these are averaged over 5 points. Above 94 km all points (22 measurements per set) are plotted. The lack of continuity in the plotted densities is due to the 25% duty cycle of the probe. It was disabled part of the time to eliminate interference in the cross modulation measurements. There were several instances in which the probe provided no data during an entire period of operation. These are attributable to temporary confusion of the logic circuitry which controlled the sweep.

To assess the accuracy of the probe in measuring electron density the points corresponding to $X = 1$ and $X = 1 + Y$ from the sensing wave reflection level data have been plotted in Figure 23. These are in good agreement with the probe data.

One mission of the probe was to detect changes produced by the gyrofrequency pulses. This was the reason for the fast sweep time. As was the case for the measurements of gyrofrequency antenna impedance and excitation light, the probe data also indicates no detectable modification of either electron density or temperature near the rocket. This supports the assumption of very weak gyro-interaction effects.

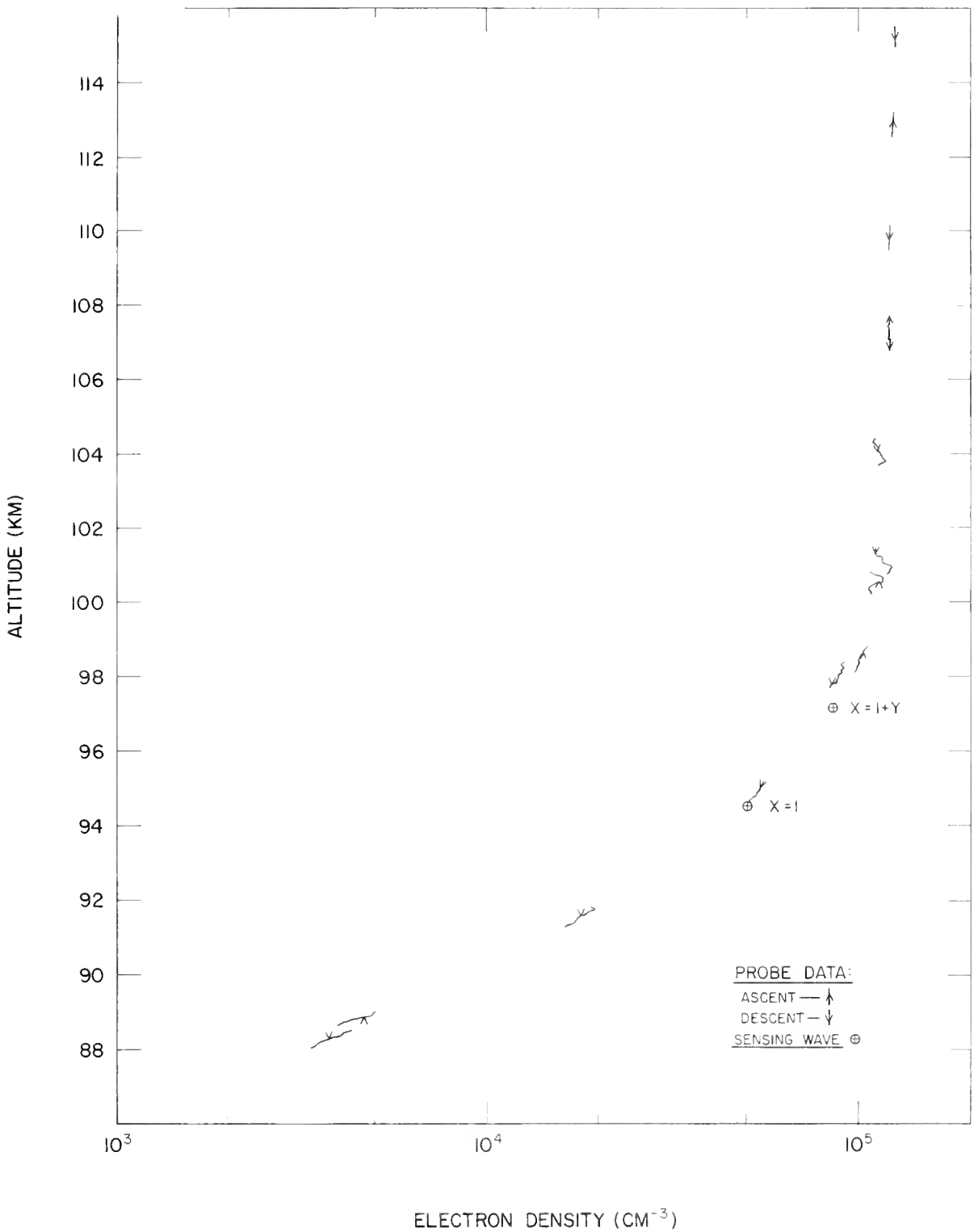

Figure 23. GIRE-II electron density profile from real impedance probe and sensing wave reflection.

6. CONCLUSIONS

The two gyro-interaction experiments have shown that the electron energy and density distributions near a rocket in the lower ionosphere can be detectably altered by the emission of gyrofrequency energy from the rocket. Immediately following each brief gyrofrequency pulse the rocket was at the center of such a disturbed region. The altered quantities then began to return to their equilibrium states, and the rates at which these processes tock place were deduced from cross-modulation of a sensing wave which had traversed the disturbance.

In the first experiment, GIRE-I, cross-modulation of the sensing wave below 65 km was attributed to excess electrons generated by ionization near the gyrofrequency antennas. The shapes of the individual cross-modulation wave forms were related to the rate of removal of excess electrons due to attachment. It was noted that at each altitude the ratio of the attachment rate obtained from this experiment to the molecular density is approximately a constant. This indicates the removal of electrons by a two-body process. The rates, however, are too large to be attributed to either two- or three-body radiative attachment to molecular oxygen. It has been generally accepted that the latter is the dominant electron removal process near 60 km, which, however, implies that the density of ions at this altitude should be an order of magnitude less than has been determined by several experimenters. This factor supports the present attachment rate measurements although the process is not known.

A study of weak gyro-interaction effects was made with the GIRE-II experiment. Here cross-modulation of the sensing wave was related to the rate of loss of excess electron energy, $G\nu$. Values of $G\nu$ obtained in this manner in the range of 92 to 97 km are in good agreement with an extrapolation of the

data of Fejer[4]. While the rocket was in the region of the ionosphere where energy at the sensing wave frequency (2.02 Mc) could not propagate an intense plasma, noise of unknown origin was detected. It was noted that each gyrofrequency pulse produced cross modulation of the noise; this showed the unexpected result that the noise input to the receiver decreased with increasing electron temperature. The utility of the frequency dependence of the real part of the impedance of a short dipole in measuring electron density and collision frequency was also demonstrated in this experiment.

As is the case in much ionospheric research which uses rockets, the high costs involved prohibit the exhaustive experimentation common to laboratory endeavors. It is recognized that each result inferred from the GIRE data is only representative of an isolated experiment; hence, these have been presented with some degree of inconclusiveness. However, the practicality of in situ measurements of the rate coefficients for electron attachment and for the loss of excess electron energy has been demonstrated.

The results obtained in these experiments will also be useful in refining the measurement techniques for future rocket experiments. Current plans include an experiment, to be launched early in 1965, in which attachment rates will be measured by two means and the results compared. The data will be obtained from cross-modulation during ascent (similar to GIRE-I) and from a probe technique during descent. In the latter, excess electrons generated by ionization near a gyrofrequency antenna will, as the payload moves, subsequently be detected by several probes towed in the wake of the rocket. With knowledge of the rocket velocity the attachment rate can be determined from these data. To insure that the probes follow in the wake, they are to be fastened at various points along a cord which joins a drag device (similar to a parachute)

to the rocket. It is also contemplated that a separate probe will be instrumented to study the mean fraction of energy lost by an electron per collision, G, in the ionosphere. This coefficient is to be deduced from the nonlinear behavior of the real part of the admittance of a short dipole as a function of applied RF voltage.

BIBLIOGRAPHY

1. B.D.H. Tellegen, "Interactions Between Radio Waves," Nature, Vol. 131, p. 840 (1933).

2. V. A. Bailey and D. F. Martyn, "The Influence of Electric Waves on the Ionosphere," Phil. Mag., Vol. 18, p. 369 (1934).

3. V. A Bailey, R. A. Smith, K. Landecker, A. J. Higgs, and F. H. Hibberd, "Resonance in Gyro-Interaction of Radio Waves," Nature, Vol. 169, p. 911 (1952).

4. J. A. Fejer, "The Interaction of Pulsed Radio Waves in the Ionosphere," J.A.T.P., Vol. 7, p 322 (1955).

5. J. A. Fejer and R W Vice, "An Investigation of the Ionospheric D-Region," J.A.T.P., Vol. 16, p. 291 (1959).

6. G. - C. Rumi, "Experiment Luxembourg Cross Modulation at High Latitude, Low Height," IRE Trans. on Antennas and Propagation, Vol. AP-10, p 594, (1962).

7. L. Goldstein, J M Anderson, and G. Clark, "Interaction of Microwaves Propagated through a Gaseous Discharge Plasma," Phys Rev., Vol. 90, p. 151 (1953).

8. K V. Narasinga Rao, J T. Verdeyen, and L Goldstein, "Interaction of Microwaves in Gaseous Plasmas Immersed in Magnetic Fields," Proc. IRE, Vol. 49, p. 1877 (1961).

9. V. A Bailey, "On Some Effects Caused in the Lower Ionosphere by Electric Waves," Phil Mag., Vol. 26, p. 425 (1938)

10. M. Curolo, "Effects of Radio Gyrointeraction and Their Interpretation," Nature, Vol. 166, p 98 (1950).

11. S F Singer, E. Maple, and W. A Bowen, "Evidence for Ionospheric Currents from Rocket Experiments Near the Geomagnetic Equator," Journal of Geophysical Research, Vol. 56, p. 265 (1951).

12 H A Shubert, private communication.

13. "A Study of Processes in the Ionosphere by Means of Gyro-Interaction Experiments Carried Out with Rockets," Final Report, Contract AF19(604)-5565, Antenna Laboratory and Gaseous Electronics Laboratory, Department of Electrical Engineering, University of Illinois, Urbana (1962).

14. T. E. Shelton, "Aerobee AJ 10-25 (AA1.193) Vertical Probe Launching Report," Office of Aerospace Research, AIDR No 62-20 (1962).

15 G. A. Deschamps, "Scattering Diagrams in Electromagnetic Theory," Symposium on Electromagnetic Theory and Antennas, Copenhagen (1962).

16 R. F. Harrington, Time-Harmonic Electromagnetic Fields, (McGraw-Hill Book Co., New York, 1961)

17. A V. Gurevich, "On the Effect of Radio Waves on the Properties of Plasma," Sov Phys. JETP, Vol 3, p 895 (1957)

18 P. A. Minzner, K W. Champion, and H. Pond, "The 1959 ARDC Model Atmosphere," Air Force Surveys in Geophysics, No. 115, AFCRC, 1959.

19 P J Nawrocki and R Papa, Atmospheric Processes, (Prentice Hall, New Jersey 1963)

20 M Nicolet and A C Aikin, "The Formation of the D Region of the Ionosphere," Journal of Geophysical Research, Vol 65, p. 1469 (1960)

21 D S Burch, S J Smith, and L M Branscomb, "Photodetachment of O_2^-," Phys Rev., Vol 112, p 171 (1958)

22 R E Bourdeau, J Chapman and K Maeda, "Ionospheric Research by Means of Rockets and Satellites," presented at the 14th General Assembly of URSI, Tokyo, Japan (1963)

23. R. C. Sagalyn and M. Smiddy, "Rocket Investigation of Electrical Structure of the Lower Ionosphere," Space Research IV (1963).

24. L. G. Smith, "Rocket Measurements of Electron Density and Temperature in the Nighttime Ionosphere," AGU First Western National Meeting, Los Angeles (1961).

25. E. C. Whipple, Jr., "Electricity in the Terrestrial Atmosphere Above the Exchange Layer," Third International Conference on Atmospheric and Space Electricity,Montreaux, Switzerland (1963).

26. R. L. DeCosmo, "Aerobee 150 (AC3.607) Vertical Probe Launching Report," Office of Aerospace Research, AIDR No. 63-54 (1963).

27. W. P. Allis, S. J. Buchbaum, and A. Bers, Waves in Anisotropic Plasmas (The MIT Press, Cambridge, Mass., 1963).

28. K. Balmain, "The Impedance of a Short Dipole Antenna in a Magnetoplasma," Ph.D. Thesis, Department of Electrical Engineering, University of Illinois, Urbana (1963).

29. D. M. Schlapp, "Some Measurements of Collision Frequency in the E-Region of the Ionosphere," J.A.T.P., Vol. 16, p. 340 (1959).

30. V. L. Ginzburg and A. V. Gurevich, "Nonlinear Phenomena in a Plasma Located in an Alternating Electromagnetic Field," Soviet Physics Uspekhi, Vol. 3, p. 115 (1960).

31. K. Takayama, H. Ikegami, and S. Miyazaki, "Plasma Resonance in a Radio Frequency Probe," Phys. Rev. Letters, Vol. 5, p. 238 (1960).